Aicumene:2026.042v2 [q-bio.NC] October 24, 2026

Brain Oscillator Intrinsic Dimension marks consciousness, recovery mode, and failed downshifting in coma

Alexandra Bernadotte*, Ivan Menshikov

Aicumene.†

*Corresponding author. Email: bernadotte@aicumene.com

These authors contributed equally to this work.

Aicumene preprint 2026.042v2 · Working paper, version 2 · October 24, 2026

Version 1 (July 2026): Aicumene:2026.042v1, doi:10.13140/RG.2.2.31610.25288. A clinically focused version of this manuscript is under peer review; this preprint reports the same analyses and adds the section *Beyond the brain*.

Brain function may depend less on maximizing complexity than on controlling how many dynamical degrees of freedom are active at a given time. Here we introduce brain oscillator intrinsic dimension (BOID), a geometrically grounded measure of the number of resolved oscillatory degrees of freedom in multichannel neural time series, linking finite-mode Hankel geometry to explicitly resolved dynamical modes.

Across human and mouse sleep, propofol anesthesia, expert meditation, and post-anoxic coma, BOID revealed a common principle of regulated oscillator dimensionality. In intact brains, sleep and anesthesia were accompanied by an

†Aicumene: `https://aicumene.com`; this paper: `https://research.aicumene.com/papers/boid-coma/`.

© 2026 Alexandra Bernadotte and Ivan Menshikov. Licensed under CC BY-NC-ND 4.0.

Aicumene:2026.042v2 [q-bio.NC] October 24, 2026

organized contraction of the active oscillator repertoire. Human slow-wave sleep showed the deepest dimensional downshift, together with reduced estimator dispersion, lower spectral entropy, and simplified trajectory topology; the sleep-related contraction was reproducible across individual recordings and across species. Propofol produced a similar reduction despite prominent organized alpha activity, indicating that oscillator dimensionality is distinct from spectral power alone. Expert meditation further showed that reduced dimensionality can coexist with preserved waking control, demonstrating that low BOID is not intrinsically a marker of impaired consciousness.

Severe post-anoxic injury revealed the opposite regime. In 575 patients from the PhysioNet I-CARE cohort, poorer outcome was associated with increased oscillator dimensionality and pathological mode proliferation. A pathological mode-proliferation index reached an AUC of 0.77, while a multimodal model combining oscillator, intrinsic-dimensional, spectral, burst-suppression, and clinical features reached an internally cross-validated AUC of 0.81. Because post-cardiac-arrest outcomes can be confounded by EEG-informed withdrawal of life-sustaining therapy, these associations should not be interpreted as direct measures of biological recoverability.

Together, these results support regulated oscillator dimensionality as a structural principle of brain-state organization: intact neural systems expand and contract their active dynamical repertoire according to state, whereas severe injury can disrupt this regulation and produce pathological mode proliferation. The critical variable may therefore be not complexity itself, but control over dynamical dimensionality.

BOID is defined for any multivariate time series with finite oscillatory structure, not only for brain recordings. We outline how the same estimator applies to economic and financial time series as a regime read-out, to multivariate data analysis as a model-order criterion, and to the structural assessment of artificial intelligence, where it supplies the dynamical component of the intrinsic-dimension criterion for strong intelligence.

Aicumene:2026.042v2 [q-bio.NC] October 24, 2026

Introduction

A suppressed electroencephalogram (EEG) is often read as a sign of a failing brain. In comatose survivors of cardiac arrest, low-voltage, slowed, discontinuous, burst-suppressed, seizure-like, or rhythmic-periodic EEG patterns enter formal neurological prognostication and can influence decisions to continue or withdraw life-sustaining therapy[28, 26, 34]. Yet the inference from suppression to irreversibility is not secure. The same macroscopic suppression is produced by brains that are known to recover: deep slow-wave sleep and general anesthesia both reduce cortical activity and conscious access, but full consciousness can return within minutes to hours [1, 2]. Suppression is therefore neither sufficient for irreversible injury nor absent from ordinary physiology. The critical question is not whether the EEG is quiet, but whether the quiet state is dynamically organized enough to be recoverable.

This distinction matters because coma prognostication is not an ordinary supervised-learning problem. In post-anoxic coma, the observed outcome is not an independent ground truth: EEG contributes to the decision to withdraw life-sustaining therapy, and withdrawal can produce the poor outcome that is later used to validate the EEG marker[29, 28]. A patient judged unrecoverable may be withdrawn and recorded as a poor outcome, closing a self-fulfilling prognostic loop. Under this confound, false pessimism is structurally difficult to detect: the missing datum is the counterfactual of what would have happened had support been continued despite a pessimistic EEG. Thus, retrospective coma cohorts can test association with observed outcome, but they cannot by themselves establish biological irrecoverability.

We propose that the relevant variable is not the depth of suppression, nor complexity as a monotonic quantity, but the organization of the residual dynamics. A quiet but intact brain should generate few but coherent oscillatory modes: a low-dimensional, well-structured trajectory. A brain that has lost dynamical control should instead show disorganization, fragmentation, or unstable mode proliferation, even if the EEG appears globally suppressed. This leads to a broader theory of regulated oscillator dimensionality: healthy brains do not maximize complexity; they expand and contract their active oscillator repertoire according to state. High dimensionality can support conscious engagement in the intact brain, low dimensionality can support recovery or trained efficiency, and high dimensionality can become pathological after injury when it reflects fragmented

Aicumene:2026.042v2 [q-bio.NC] October 24, 2026

mode proliferation rather than richer conscious dynamics.

To test this idea, we introduce brain oscillator intrinsic dimension (BOID), a geometric read-out of the number of active oscillatory modes generating a multichannel brain recording. The method extends topology-driven time-series classification and Hankel-embedded brain-signal modeling, in which delay-embedding geometry and intrinsic dimension are treated as invariants of the underlying dynamics [3, 9, 5, 7, 8]. A recording is embedded as a block-Hankel trajectory and represented as a finite superposition of exposinusoidal components. Multichannel singular spectrum analysis (MSSA) [6], followed by ESPRIT pole extraction, estimates the active modes; their count defines BOID [3, 7, 8, 10, 4]. We pair this scalar oscillator count with measures of dynamical organization, including estimator dispersion, spectral entropy, Hankel-spectrum structure, and trajectory topology [18, 19, 20, 21]. BOID is distinct from spectral power: band power asks how much signal energy lies in predefined frequency bands, whereas BOID asks how many dynamically independent oscillatory modes are needed to generate the observed signal. BOID is related to oscillator and minimum-description-length views of brain dynamics, but differs from both predefined oscillator-population models and microscopic spiking models because it estimates the effective mesoscopic oscillatory description directly from data [11, 12, 13, 14, 15, 16]. BOID is also distinct from generic signal complexity, because it counts structured oscillatory degrees of freedom rather than raw irregularity or noise-dominated unpredictability.

We first establish the geometry of recoverable suppression in states where reversibility is known. In human sleep, mouse sleep, and propofol anesthesia, low-activity brain states were not merely low-dimensional; they were organized [17, 23, 22, 24]. Deep slow-wave sleep showed the lowest oscillator dimension, low dispersion among independent intrinsic-dimension estimators, low spectral entropy, and simple trajectory topology. Propofol anesthesia provided a pharmacological test of the same principle [24], and expert meditation showed that low dimensionality is not pathological by itself: trained waking control can also operate with a reduced dynamical repertoire[25]. These intact-brain states define an organized-suppression signature: few coherent modes, low estimator disagreement, and clean low-dimensional geometry.

We then ask whether this signature transfers to post-anoxic coma. Here the answer is deliberately cautious. In PhysioNet I-CARE, poorer outcomes trended toward greater dynamical disorganization and higher oscillator-mode proliferation, and Hankel/MSSA signal-subspace geometry carried

Aicumene:2026.042v2 [q-bio.NC] October 24, 2026

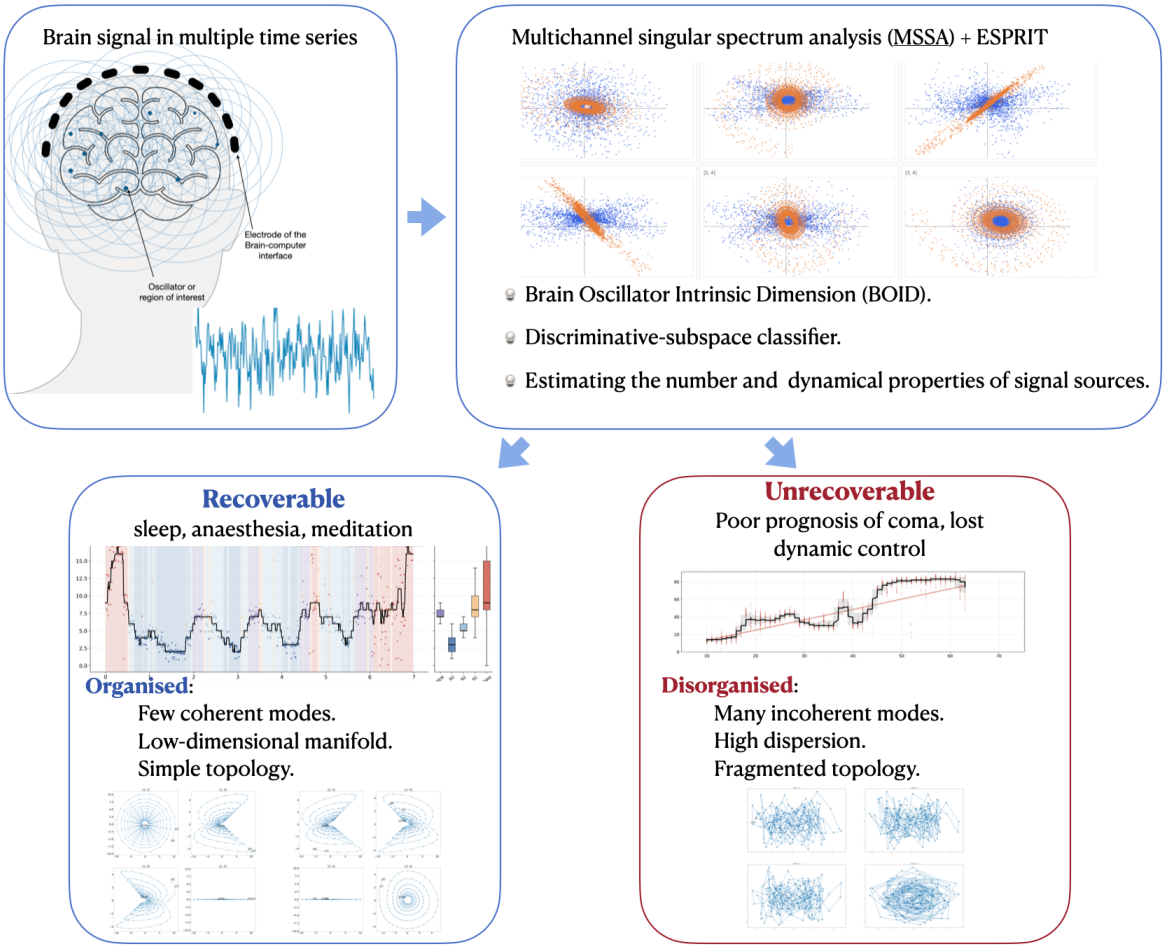

Figure 1: **Suppression is not irreversibility: BOID and organization distinguish recoverable low-activity states from pathological loss of dynamical control.** Brain oscillator intrinsic dimension (BOID) estimates the number of active oscillatory modes recovered from multichannel Hankel embeddings by MSSA and ESPRIT pole estimation, and is paired with estimator-dispersion, spectral-entropy, and topological measures of organization. Recoverable suppression (deep sleep, anesthesia, and controlled low-dimensional waking states) is low-dimensional yet organized, whereas pathological loss of dynamical control produces fragmented or unstable activity.

Aicumene:2026.042v2 [q-bio.NC] October 24, 2026

outcome-associated information [26, 27, 30]. However, the sleep-defined organized-suppression axis separated outcomes only weakly in short retrospective recordings, and all coma outcome associations remain confounded by EEG-informed withdrawal of life support [29, 28]. We therefore do not claim that the present retrospective data identify which comatose patients are recoverable. Instead, the coma analysis exposes the central validation problem: the marker that matters clinically cannot be validated against labels partly produced by the same class of signals.

The resulting contribution is threefold. First, we identify organized low-dimensional dynamics as a geometric signature of recoverable brain-state suppression in intact brains. Second, we place this signature within a theory of regulated oscillator dimensionality, in which healthy brain function depends on controlled expansion and contraction of the active oscillator repertoire. Third, we show why retrospective coma datasets cannot settle whether a suppressed EEG is irreversible, and specify the prospective withdrawal-blind or withdrawal-delayed validation needed to test whether organized-suppression geometry can identify recoverable coma states. The clinically relevant information may lie not in the depth of EEG suppression, but in the organization of the dynamics that remain. See Fig. 1. Fourth, because the estimator is defined for any multichannel time series generated by a finite set of damped oscillatory modes, we outline (section *Beyond the brain*) how BOID transfers to economic and financial series, to multivariate data analysis, and to the structural assessment of artificial intelligence, where it provides the dynamical component of the intrinsic-dimension criterion for strong intelligence proposed in Ref. [40] and has already been applied to the latent dynamics of trained neural networks in a companion study [41].

Results

Recoverable suppression in sleep is organized, not disorganized

Sleep provided the first within-brain test of whether suppression reflects loss of dynamical control or organized recovery. In Sleep-EDF Expanded recordings [17], BOID decreased with sleep depth across 10 subjects, 5,535 four-second windows, and 56,282 extracted oscillatory modes. Subject-level median BOID declined from wakefulness to N1, N2, and N3 slow-wave sleep (18, 13, 8, and 4 modes, respectively), with REM in an intermediate regime (11 modes; Kruskal–Wallis

Aicumene:2026.042v2 [q-bio.NC] October 24, 2026

$H = 43.0$, $p = 1.0 \times 10^{-8}$). Whole-night trajectories showed that dimensional downshifts aligned with transitions into deeper non-REM sleep and reversed during REM or wake transitions (Fig. 2A). Thus, physiological sleep is not merely reduced activity; it is a reversible contraction of the active oscillator repertoire into a low-dimensional brain state.

The sleep effect was not specific to the BOID extraction pipeline. Independent estimators from fractal, nearest-neighbor, graph, and topological families converged on the same conclusion: scalar dimensionality was lowest in N3 slow-wave sleep. Correlation dimension, false-nearest-neighbor dimension, Higuchi fractal dimension, minimum-spanning-tree length, and Brito–Quiroz–Yukich degree all reached minima in N3, whereas first-homology loop descriptors peaked in REM, separating scalar dimensionality from cyclic trajectory richness [18, 19, 20, 21] (Fig. 2E). REM therefore remained relatively low-dimensional by scalar measures but topologically richer, whereas N3 combined low dimension with simple trajectory structure.

Crucially, the deepest recoverable suppressed state was not disorganized. N3 slow-wave sleep, the physiological state that most closely resembles clinical EEG "suppression," showed the lowest oscillator dimension together with the most coherent dynamics: the dispersion among independent intrinsic-dimension estimators fell from a median of 4.6 in wakefulness to 1.1 in N3, spectral entropy from 53 to 22, and the participation ratio from 8.3 to 4.4 (Fig. 2B,C). As the intact brain entered its deepest reversible suppression, it therefore produced fewer but more coherent modes, with independent estimators converging on a clean low-dimensional organization. This defines an *organized-suppression signature*: low oscillator dimension together with low estimator dispersion, low spectral entropy, and simple topology. We use this signature as the reference geometry of a quiet but intact brain.

A supporting cross-species analysis in 92 mice from the OpenNeuro Mouse Sleep Staging Validation dataset (ds006366) showed the same direction despite differences in species, montage, and sampling conditions [23]. Because sleep-stage labels in this dataset were encoded numerically and not fully documented, the mouse analysis is treated as supporting replication rather than as a primary test of the theory. BOID decreased from wakefulness to non-REM sleep and returned toward wake/REM levels, with a highly significant stage effect ($p = 1.7 \times 10^{-11}$; Fig. 2D). Thus, the low-dimensional sleep state is not specific to human Sleep-EDF scoring or montage, but appears across mammalian sleep recordings.

Aicumene:2026.042v2 [q-bio.NC] October 24, 2026

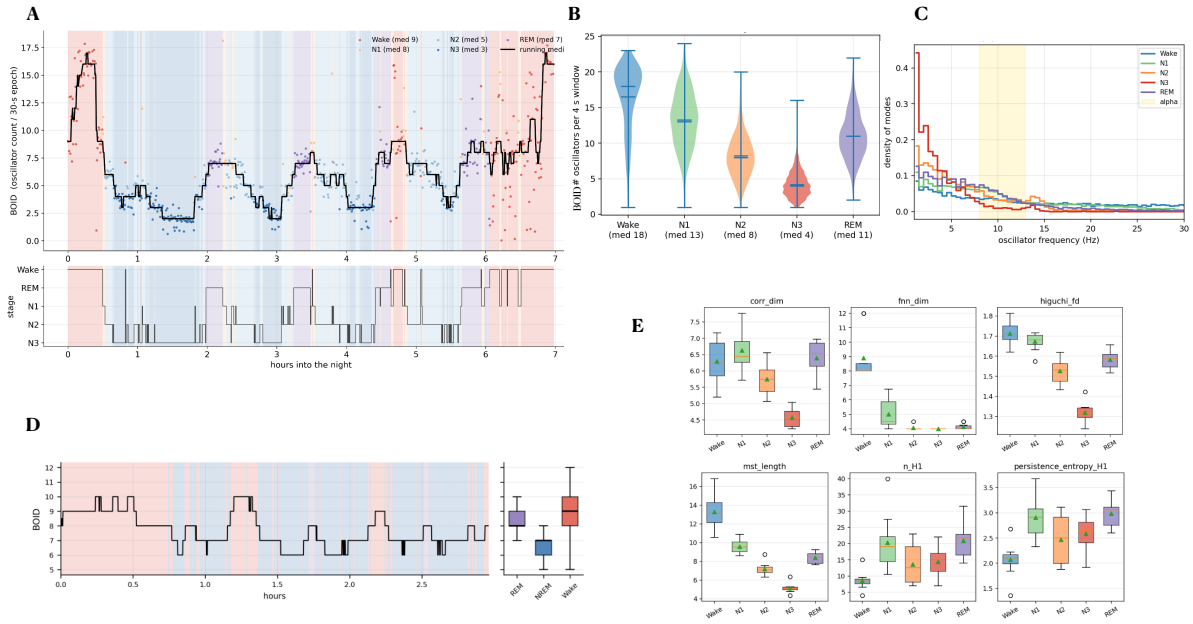

Figure 2: **Recoverable suppression in sleep is low-dimensional and organized in human and mouse.** **(A) BOID follows sleep architecture across a whole night in human.** In the representative Sleep-EDF recording SC4001, BOID tracked the hypnogram, remaining highest in wakefulness, lowest in N3 slow-wave sleep, and intermediate in REM and N1. **(B) BOID decreases with sleep depth in human sleep.** Across Sleep-EDF stages, BOID is highest in wakefulness, decreases through non-REM sleep, and reaches a minimum in N3, with REM occupying an intermediate regime. **(C) Sleep-related BOID reduction is distinct from spectral power.** Sleep depth is accompanied by both spectral reorganization and a reduction in oscillator dimensionality, indicating that BOID captures the size of the active oscillator repertoire rather than the power of a single frequency band. **(D) Cross-species validation in mouse sleep.** In OpenNeuro ds006366, mouse EEG reproduced the human pattern, with BOID lowest in non-REM sleep and higher in wakefulness and REM. Delta and theta power supported the physiological identification of the stage codes. **(E) Independent estimators confirm the deep-sleep dimensional minimum.** In Sleep-EDF, independent fractal, graph-based, and nearest-neighbor estimators also identified N3 as the lowest-dimensional sleep stage, whereas topological loop descriptors peaked in REM, separating scalar dimensionality from cyclic trajectory structure.

Aicumene:2026.042v2 [q-bio.NC] October 24, 2026

An independent in-house dataset provided a further validation on wearable hardware. In 40 participants recorded with the Aicumene non-invasive EEG neurointerface platform, which was not used to derive the BOID framework or tune any analysis parameters, subject-level median BOID declined from wakefulness to N1, N2, and N3 slow-wave sleep (17, 12, 8, and 4 modes, respectively), with REM in an intermediate regime (10 modes; Kruskal–Wallis $H = 40.0$, $p = 4.3 \times 10^{-8}$). This reproduced the Sleep-EDF ordering and supports the generalization of sleep-related dimensional downshifting to wearable neurointerface recordings.

Propofol anesthesia is pharmacological dimensional downshifting

Propofol anesthesia provided an independent pharmacological test of whether reversible loss of consciousness is accompanied by organized contraction of the active oscillator repertoire. In OpenNeuro ds005620, a repeated-awakening study with 21 healthy adults and 65-channel EEG [24], BOID fell within subjects from wakefulness to sedation (median 30.5 to 21.5 modes; paired Wilcoxon $p = 3.2 \times 10^{-3}$, $n = 20$; Fig. 3A). Thus, reversible pharmacological suppression, like deep sleep, was associated with a lower-dimensional brain-state geometry.

This effect was not reducible to conventional spectral power. Propofol sedation occurred together with the canonical organized alpha signature, showing that a brain state can have strong band-limited rhythmic activity while remaining low-dimensional. Band power measures energy within predefined frequency ranges; BOID estimates the number of dynamically independent oscillatory modes required to generate the signal. In the sedated awakenings, BOID did not reliably separate report from no-report trials, suggesting that it reflects the global anesthetic state more strongly than momentary reportability in this dataset. Propofol therefore supports the same principle observed in sleep: recoverable suppression is not simply low activity, but a structured reduction of dynamical degrees of freedom.

Expert meditation is low-dimensional waking efficiency

Low BOID is not pathological by itself. The Brandmeyer–Delorme meditation dataset [25] provided a waking control case in which reduced dimensionality occurred without loss of function. Momentary concentration and mind-wandering did not reliably change BOID. Instead, meditation

Aicumene:2026.042v2 [q-bio.NC] October 24, 2026

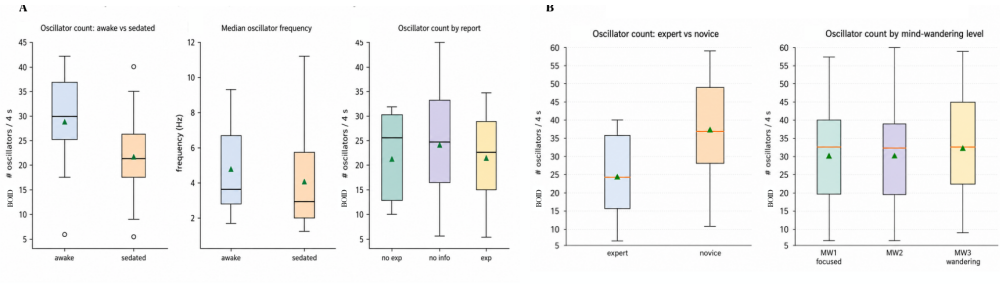

Figure 3: **Low-dimensional brain-state geometry occurs in reversible anesthesia and expert waking control.** **(A) Propofol sedation reduces BOID.** BOID decreases from wakefulness to sedation in healthy adults despite organized propofol alpha activity. This dissociation shows that BOID is not a band-power measure, but a marker of the size of the active oscillator repertoire. **(B) Meditation expertise lowers intrinsic dimension.** Expert meditators show lower BOID and related intrinsic-dimension estimates than novices, whereas momentary mind-wandering does not strongly change the geometry. Low dimensionality can therefore reflect efficient waking control rather than collapse.

expertise was associated with lower intrinsic dimension across the estimator battery: correlation dimension, false-nearest-neighbor dimension, Levina–Bickel estimate, singular-spectrum entropy, and BOID all shifted downward in expert meditators relative to novices (Fig. 3B). Expert meditation therefore appears to be a low-dimensional waking efficiency regime, in which trained control is maintained with fewer active dynamical degrees of freedom.

Together, propofol and meditation sharpen the interpretation of BOID. Low dimensionality is not a generic marker of impaired brain function. In reversible anesthesia it marks pharmacological downshifting; in expert meditation it may mark efficient waking control. The meaning of dimensionality is therefore context-dependent: the same reduction in active oscillator repertoire can reflect recovery, suppression of conscious access, or trained control, depending on the organization and biological state in which it occurs.

Coma reveals pathological mode proliferation, but recoverability cannot be validated retrospectively

Post-anoxic coma is the pathological setting in which the distinction between organized and disorganized suppression matters most. Sleep and anesthesia show that an intact brain can reduce

Aicumene:2026.042v2 [q-bio.NC] October 24, 2026

conscious access by entering an organized low-dimensional state. If a comatose brain displayed the same organized-suppression geometry, its quiet EEG might reflect a recoverable state rather than irreversible injury. Conversely, if the injured brain fails to downshift into a coherent low-dimensional regime, apparent suppression may coexist with fragmentation, unstable mode proliferation, or loss of dimensional control.

We analyzed all available comatose survivors of cardiac arrest in PhysioNet I-CARE [26, 27]: 575 patients and 826 recordings at 24–72 hours after arrest, dichotomized into Good (CPC 1–2) and Poor (CPC 3–5) neurological outcome. In this injured-brain context, high BOID marked worse observed outcome rather than preserved consciousness. A pre-specified pathological mode-proliferation index (PMPI), combining high mode count, high-frequency poles, burst intermittency, and mode-frequency entropy, was elevated in poor-outcome patients (AUC 0.77, one-sided Mann–Whitney $p < 10^{-3}$); bare BOID showed the same direction (AUC 0.68, $p < 10^{-5}$), at both 24 and 72 hours. At 72 hours, the BOID distribution was shifted upward in Poor-outcome patients, and the time-resolved patient matrix showed heterogeneous but outcome-associated oscillator-dimensional trajectories (Fig. 4A,B).

This result separates two questions that should not be conflated. The first is whether a coma EEG resembles the organized low-dimensional geometry of recoverable suppression defined by sleep and anesthesia. The second is whether the injured brain shows pathological dimensional dysregulation associated with poor observed outcome. The present retrospective data support the second claim more strongly than the first. Higher BOID and PMPI indicate that the poor-outcome injured brain often does not simply become low-dimensional and silent; rather, it can enter a fragmented, high-dimensional regime of unstable mode proliferation. Thus, after anoxic injury, high oscillator dimensionality should not be interpreted as richer conscious dynamics, but as a candidate marker of failed dimensional regulation.

The reason this distinction matters is that recoverability cannot be validated retrospectively in the usual way. Neurological outcome in post-anoxic coma is not an independent biological ground truth: a large share of deaths follow withdrawal of life-sustaining therapy, and those withdrawal decisions are themselves informed by EEG-based prognosis [29, 28]. A patient judged unrecoverable may be withdrawn and then recorded as a poor outcome, closing a loop in which an EEG-derived marker is validated against decisions it helped to make. Under this self-fulfilling-prophecy confound, a marker

Aicumene:2026.042v2 [q-bio.NC] October 24, 2026

that correctly identified a salvageable patient would be scored as wrong whenever that patient was nonetheless withdrawn. False pessimism is therefore structurally invisible in retrospective labels.

For this reason, no reanalysis of I-CARE and no larger retrospective cohort can by itself establish whether an organized-suppression marker identifies biological recoverability. Retrospective data can test association with observed outcome, but not the missing counterfactual: what would have happened had support been continued despite a pessimistic EEG. Our coma results should therefore not be read as evidence that current prognostication errs, which we cannot show. They should be read as evidence that oscillator-dimensional geometry carries outcome-associated information while the clinically central question—whether a suppressed EEG is recoverable or irreversible—requires prospective withdrawal-blind or withdrawal-delayed validation.

Beyond scalar BOID, the geometry of the early-EEG signal subspace also carried withdrawal-confounded outcome information. We tested a Bernadotte discriminative-subspace classifier based on the same Hankel/MSSA geometry underlying BOID. Each multichannel recording was embedded into a block-Hankel trajectory, reduced to its leading MSSA signal subspace, and represented by the corresponding subspace projector. The classifier compared class mean projectors for Good and Poor outcomes and retained only the low-dimensional discriminative directions of their difference operator [3, 7, 8]. This approach does not rely on oscillator count alone; it uses the orientation of the reconstructed signal subspace as a complementary geometric read-out of brain-state organization.

In 500 patients using the first 24 hours of EEG, the class-separation operator had a spectrum concentrated in a few Good- and Poor-characteristic directions. Restricting the classifier to this discriminant subspace yielded a standalone out-of-fold AUROC of 0.724 and balanced accuracy of 0.670 in the displayed setting ($r = 12$, $k = 6$; Fig. 4E). The discriminative projection showed partial class separation (Fig. 4F), and the spectrum of $\Delta = P_{\text{Good}} - P_{\text{Poor}}$ contained a large near-zero shared bulk with a small number of extreme Good- and Poor-associated directions (Fig. 4G). Thus, the outcome-associated signal appears at two levels: scalar proliferation of oscillatory modes and the orientation of the reconstructed Hankel/MSSA signal subspace. As for every coma association in this study, however, both predict a withdrawal-influenced outcome and therefore index current prognostic practice rather than ground-truth recoverability.

We next fused four feature families: BOID, the intrinsic-dimension battery, spectral and burst-suppression descriptors, and routine clinical variables. Under outcome-stratified, patient-grouped

Aicumene:2026.042v2 [q-bio.NC] October 24, 2026

five-fold cross-validation, BOID alone reached AUC 0.68; spectral and burst descriptors reached 0.69; the intrinsic-dimension battery reached 0.72; clinical variables alone reached 0.72; BOID plus the intrinsic-dimension battery reached AUC 0.74; adding spectral and burst descriptors reached 0.77; and the full model including clinical variables reached AUC 0.81 (Fig. 4C). ROC analysis showed that the full multimodal model outperformed the modality-stack baseline and identified a subset of poor-outcome patients at the conservative false-positive-rate operating region FPR $\leq 5\%$ (Fig. 4D). These values are internal patient-grouped cross-validation results, not hidden-test challenge scores, and the predicted endpoint is withdrawal-confounded observed outcome rather than biological recoverability.

Representative single-patient trajectories illustrate the same interpretation. In a Good-outcome example, BOID remained relatively low and stable with a transient fluctuation, whereas in a Poor-outcome example BOID increased over time, consistent with pathological mode proliferation (Fig. 4H). These examples are illustrative only: individual trajectories overlap across patients and should not be interpreted as a recoverability rule.

These coma results expose the pathological boundary of regulated oscillator dimensionality. In intact brains, low-dimensional suppression can be organized and recoverable. In injured brains, higher apparent dimensionality can reflect pathological mode proliferation rather than preserved consciousness. Poor-prognosis coma may therefore represent failed dimensional regulation: instead of entering a coherent low-dimensional stabilization regime, the injured brain decomposes into partially independent oscillatory components. This interpretation remains a mechanistic hypothesis, not a clinical decision rule. Its confirmation requires full-recording analyses and prospective validation in cohorts where the candidate marker is blinded from treating clinicians or tested under a pre-specified withdrawal-delayed protocol.

Published coma-outcome models differ in input duration, artifact curation, access to ECG and clinical variables, hospital splits, hidden-test access, and operating-point tuning [30, 31, 32, 33, 34, 35, 36, 37, 38]. Our contribution is therefore not a leaderboard-topping prognostic system. It is an interpretable, data-light geometric substrate that links the same oscillator-dimensional framework used for sleep, anesthesia, and meditation to the injured brain—while showing why the clinically decisive question of recoverability cannot be answered by retrospective outcome labels alone.

Aicumene:2026.042v2 [q-bio.NC] October 24, 2026

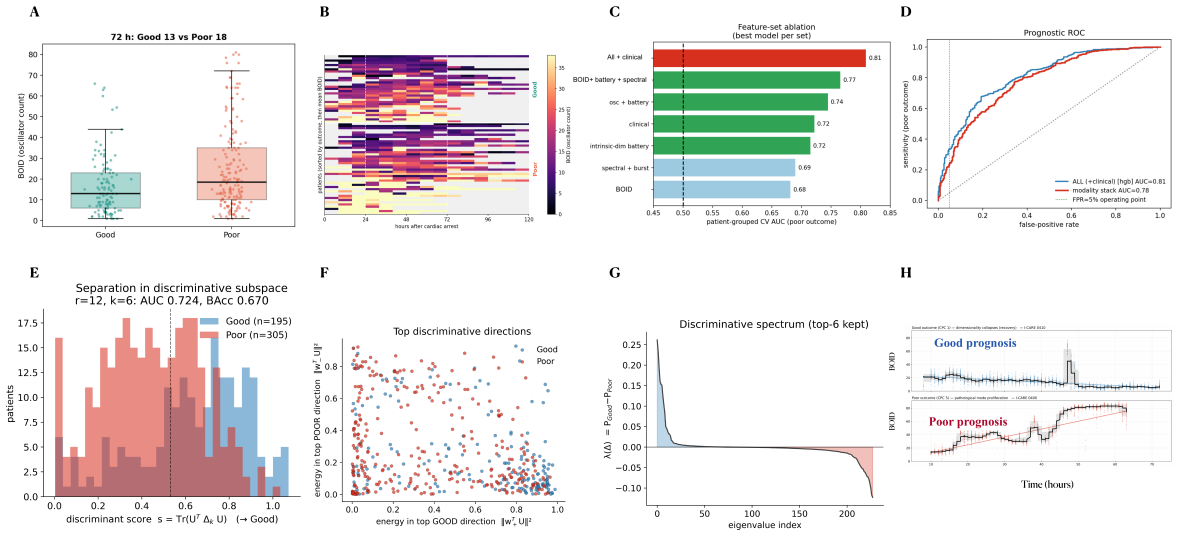

Figure 4: **Oscillator-dimensional geometry carries withdrawal-confounded outcome information after post-anoxic coma.** **(A) BOID is elevated in poor-outcome coma.** At 72 h after cardiac arrest, patients with Poor neurological outcome (CPC 3–5) show higher brain oscillator intrinsic dimension (BOID) than patients with Good outcome (CPC 1–2), consistent with pathological mode proliferation rather than preserved consciousness. **(B) Time-resolved BOID structure across patients.** Patient-level BOID trajectories across the first 24–72 h after arrest show heterogeneous temporal organization, with Poor-outcome recordings tending toward higher or more persistent oscillator-dimensional activity. **(C) Feature-set ablation.** Internal patient-grouped cross-validated AUC increases from BOID alone to intrinsic-dimension, spectral/burst, and clinical feature combinations, reaching AUC 0.81 for the full model. **(D) ROC analysis.** The full multimodal model outperforms the modality-stack baseline. The dotted vertical line marks the conservative operating region at FPR $\leq$ 5%. These are internal cross-validation results, not hidden-test challenge scores. **(E) Discriminative-subspace separation.** A Hankel/MSSA discriminative-subspace classifier separates Good and Poor outcomes using the signed score $s = \mathrm{Tr}(U^\top \Delta U)$, where $\Delta = P_{\mathrm{Good}} - P_{\mathrm{Poor}}$; the displayed setting reaches AUROC 0.724 and balanced accuracy 0.670. **(F) Good- and Poor-associated subspace directions.** Projection of patient recordings onto leading Good- and Poor-associated directions shows partial separation, indicating that outcome-associated information is present in the orientation of the reconstructed signal subspace, not only in scalar BOID. **(G) Discriminative spectrum.** The spectrum of Δ contains a large near-zero shared bulk and a small number of extreme class-associated directions, supporting a low-dimensional geometric read-out of outcome-associated EEG structure. **(H) Representative BOID trajectories.** Illustrative Good- and Poor-outcome patients show different BOID trajectories over time, but individual traces are not a recoverability rule. All panels predict observed neurological outcome, which is partly shaped by EEG-informed withdrawal-of-life-sustaining-therapy decisions. The figure therefore supports pathological oscillator-dimensional dysregulation as a withdrawal-confounded outcome signal, not as proof of biological irrecoverability.

Aicumene:2026.042v2 [q-bio.NC] October 24, 2026

Beyond the brain: BOID as a general regime read-out

Nothing in the definition of BOID is specific to neural tissue. The estimator takes a multichannel time series, forms its block-Hankel trajectory matrix, extracts the signal subspace by MSSA, resolves the subspace into damped oscillatory modes by ESPRIT, and counts the positive-frequency modes that survive the retention criteria (Methods and Supplementary Materials). The brain is the setting in which we validated the estimator against known state transitions; the construction itself applies to any system that can be approximated, over an analysis window, by a finite superposition of exposinusoidal components [3, 6, 49]. The results above establish, for such systems, three properties that make BOID useful outside neuroscience: it changes with the regime of the generating system rather than with band power alone (Fig. 2C, Fig. 3A), it agrees in direction with independent intrinsic-dimension estimators while remaining a count of structured modes rather than of irregularity (Fig. 2E), and in synthetic tests the size of the oscillator repertoire can be varied independently of noise-sensitive complexity measures (Supplementary Materials). When the estimator is applied outside neural recordings we keep the acronym and, following the companion study of trained neural systems [41], expand it as Bernadotte oscillatory intrinsic dimension; "brain" in the title of this paper names the validation setting, not the scope of the method. We sketch three applications. The third has a first empirical test in Ref. [41]; the first two are stated so that they can fail.

Economic and financial time series. Nonlinear-dynamics methods entered empirical finance through the correlation dimension: Scheinkman and LeBaron, Hsieh, and the BDS test asked whether stock returns carry low-dimensional deterministic structure and found, at best, weak and unstable evidence [45, 46, 47]. Regime structure in macroeconomic and financial series has instead been modelled statistically, most influentially by Markov-switching models in which an unobserved discrete state governs the parameters of a linear process [44]. Singular spectrum analysis has a parallel history in economics as a forecasting and decomposition tool [48, 49]. BOID sits between these traditions. It does not ask whether returns are chaotic, and it does not presuppose a fixed number of latent states; it asks how many damped oscillatory modes are needed to generate a panel of series over a window, and how that number changes over time. For a multichannel panel (sector indices, a cross-section of yields, or a set of macro indicators observed at a common frequency), BOID is computed per rolling window exactly as for an EEG montage. The regulated-dimensionality

Aicumene:2026.042v2 [q-bio.NC] October 24, 2026

principle translates into a testable prediction: periods that economists classify as regime changes should appear as contractions or expansions of the active mode count accompanied by changes in estimator dispersion and mode-frequency entropy, with the direction of change diagnostic of the regime (a contraction to few coherent modes in a crisis in which assets co-move, an expansion into many weakly coupled modes in a fragmented or liquidity-driven market). A pre-specified protocol is: daily log-returns of a fixed panel; windows of 250 trading days stepped by 21 days; the same preprocessing, retention criteria, and organization descriptors as in the Methods; comparison of the BOID trajectory with the Markov-switching state sequence estimated on the same panel. The proposal fails if the BOID trajectory is flat or uninformative across documented regime changes, or if it merely tracks realized volatility.

Multivariate data analysis and model-order selection. In any sensor array (physiological monitoring, industrial vibration, power grids, seismic or climate networks), the number of oscillatory degrees of freedom is a model-order question, and model-order selection by information criteria is known to be unstable under colored noise and closely spaced frequencies [15, 16]. The Hankel spectral rank and the ESPRIT pole count give a geometric answer that is explicitly resolved into modes with frequencies and decay rates, so that the selected order can be audited mode by mode rather than accepted as a scalar. The organization descriptors introduced here (estimator dispersion, participation ratio, mode-frequency entropy, trajectory topology) transfer unchanged and provide the same safeguard they provide in the brain: a high count with high dispersion and flat mode-frequency entropy indicates noise-driven mode proliferation, not structure. In this reading BOID is a construct-validated, interpretable model-order estimator for multivariate signals, and the sleep and anesthesia datasets serve as benchmarks in which the ground-truth direction of the order change is known.

Strong artificial intelligence. A companion paper proposes a structural, non-anthropocentric definition of levels of intelligence through intrinsic invariants of the data a system generates: intrinsic dimension, topology, and dynamical complexity, summarized in a structural profile $S(\mathcal{I}) = (\mathrm{ID}, \mathrm{Top}, \mathrm{Dyn})$ [40]. The evidence for that proposal is static: the intrinsic dimension of language-embedding clouds is close to nine across seventy languages and is lower for machine-

Aicumene:2026.042v2 [q-bio.NC] October 24, 2026

generated text [42, 43], and the intrinsic dimension of healthy human brain dynamics falls in the same range (Results). That proposal needs a validated estimator for the dynamical component, and BOID is such an estimator: it is defined on trajectories, it counts resolved degrees of freedom rather than irregularity, and the present paper shows that it tracks state regimes in a system of known strong intelligence. A companion study has taken the first step from the brain to artificial systems [41]. Applying delay embeddings, MSSA, Koopman-mode analysis, and BOID-style oscillatory dimensionality to the latent trajectories of a Continuous Thought Machine trained on maze solving, it found that learning moves input-excited modes toward the unit circle, creates functional rhythms above the aperiodic background, and separates computation into a high-dimensional desynchronized working regime and a low-dimensional synchronized resting regime; beyond the training horizon the system alternates between work and rest, replays its solution, stores the answer in accumulated synchronization, and restarts through a clock-like mode, and removing specific rotating mode pairs selectively disrupts route content or abolishes the restart clock whereas removing random planes has little effect. The result is architecture-dependent: some trained systems acquire oscillatory regimes, stores, clocks, and replay, others remain relaxation-like, line-like, or input-driven. This is the artificial counterpart of regulated oscillator dimensionality in the intact brain, and it turns the structural account into a measurement programme rather than a classification by fiat. Two applications remain open. First, hidden-state trajectories of a language model during generation form a multichannel time series (one channel per hidden unit or per principal direction) to which the same pipeline applies directly; the structural account predicts that a system approaching the level of strong natural intelligence will exhibit regulated oscillator dimensionality (expansion of the active repertoire for engaged processing, contraction for routine or consolidating phases), whereas a system that merely scales will show a repertoire that is either fixed or noise-driven, with high dispersion. Second, the regulated-dimensionality principle becomes a design target rather than only a marker: an artificial system that can enter, sustain, and leave low-dimensional organized regimes is closer to the dynamical signature of intact brains than one that maximizes complexity. Both statements are falsifiable with the estimator and descriptors defined here, and they connect the brain-state results of this paper, through Ref. [41], to the measurement protocol of Ref. [40].

Aicumene:2026.042v2 [q-bio.NC] October 24, 2026

Discussion

Together, these findings suggest that the central dynamical variable of brain state is not complexity itself, but the capacity to regulate the number of active oscillatory degrees of freedom. Brain states are not arranged along a simple axis from low to high complexity. In intact brains, the active oscillator repertoire expands and contracts according to functional demand: it is larger during engaged wakefulness, contracts during deep sleep and pharmacological suppression, and can also contract during trained waking states such as expert meditation. Low dimensionality is therefore not intrinsically pathological, just as high dimensionality is not intrinsically beneficial. What appears to distinguish intact brain dynamics is *regulated dimensional control*—the ability to enter, maintain, and leave an appropriate dynamical regime.

This distinction changes how suppressed brain activity should be interpreted. Deep sleep and general anesthesia provide direct examples in which substantial reductions of conscious access are reversible and accompanied by organized low-dimensional dynamics. In these states, dimensional contraction is not equivalent to loss of dynamical structure: it is accompanied by a restricted coherent oscillator repertoire, low estimator dispersion, reduced spectral entropy, and simple trajectory topology. The relevant distinction may therefore be not between an "active" and a "suppressed" brain, but between *organized suppression* and *loss of dimensional regulation*. A quiet brain can remain dynamically organized.

Post-anoxic coma exposed the opposite boundary of this framework. Poorer observed outcomes were associated with increased oscillator dimensionality, pathological mode proliferation, and additional outcome-associated information in the geometry of the reconstructed signal subspaces. This regime is qualitatively different from the organized dimensional contraction observed during reversible intact-brain states. In an injured brain, high dimensionality need not indicate richer information processing or preserved consciousness; it may instead reflect fragmentation, unstable recruitment of dynamical modes, and failure of the system to constrain its activity.

This leads to a more specific mechanistic hypothesis. The clinically relevant variable in coma may not be the absolute BOID value at a single time point, but whether the injured brain retains the capacity to *downshift into and sustain an organized low-dimensional regime*. Such a transition would be the dynamical analogue of the regulated suppression observed in intact recovery states.

Aicumene:2026.042v2 [q-bio.NC] October 24, 2026

Conversely, persistent mode proliferation, unstable dimensionality, or failure to enter such a regime may indicate loss of dimensional control. The present retrospective data do not establish this transition capacity as a marker of biological recoverability: the sleep-derived organization axis transferred only weakly to the short coma recordings and did not reliably separate individual outcomes. It should therefore be regarded as a prospective mechanistic hypothesis rather than as a validated clinical classifier.

This distinction is especially important because neurological outcome after cardiac arrest is not a fully independent biological ground truth. Withdrawal of life-sustaining therapy is frequently informed by neurological and EEG assessment, so an EEG-derived prognostic marker can become entangled with the decision pathway that determines the recorded outcome. A patient judged unlikely to recover may undergo withdrawal and subsequently enter the Poor-outcome class, making false pessimism intrinsically difficult to detect in retrospective data. The missing observation is counterfactual: what would have happened had support been continued despite a pessimistic neurological assessment? Under this form of incorporation and self-fulfilling-prophecy bias, prognostic accuracy alone cannot determine whether a marker predicts biological recoverability, current clinical decision-making, or some mixture of the two.

BOID is of interest in this setting because it represents a structural dynamical quantity rather than raw signal irregularity. Operationally, BOID is the number of resolved positive-frequency oscillatory modes recovered from the multichannel signal subspace within the analysis band. It therefore differs conceptually from measures of spectral spread, entropy, or algorithmic irregularity. In synthetic tests, oscillator repertoire size could be varied independently of noise-sensitive complexity measures such as Lempel–Ziv complexity and spectral entropy. This construct validity is important, but it does not solve the causal problem of coma prognostication. A mathematically well-defined and biologically interpretable marker can still be evaluated against an outcome partly produced by clinical decisions.

The appropriate next experiment is therefore not simply a larger retrospective outcome classifier. It is a prospective test of *dimensional regulation capacity*. BOID and organization descriptors should be measured continuously, or over substantially longer recordings, while remaining blinded to the treating team, or within a protocol in which withdrawal decisions are deferred for a pre-specified observation period. The key endpoint should be whether brains that subsequently recover retain, or

Aicumene:2026.042v2 [q-bio.NC] October 24, 2026

reacquire, the capacity to enter coherent low-dimensional states and transition reproducibly between dimensional regimes. Such a design would directly test whether organized dimensional downshifting contains information about biological recoverability that is not captured by conventional static prognostic descriptors.

If confirmed, this would have an important clinical implication. A suppressed EEG would no longer be interpreted primarily by the amount of residual activity, but also by whether its dynamics retain organized structure and state-transition capacity. Patients whose brains preserve such regulation could constitute a biologically distinct group even when conventional prognostic features appear unfavorable. The present data do not establish that such patients should be managed differently, nor do they identify individual patients in whom treatment withdrawal would have been inappropriate. They instead identify a concrete mechanism by which false-pessimistic prognostication could arise and define a prospective experiment capable of testing it.

The same estimator and organization descriptors are not confined to neural data. As outlined in *Beyond the brain*, they define a regime read-out for economic panels, a mode-resolved model-order criterion for multivariate signals, and the dynamical component of a structural profile of artificial intelligence. The brain-state results reported here are, in that broader programme, the validation of the estimator in a system whose regime transitions are independently known.

Several limitations remain. Absolute BOID and organization values depend on montage, sampling rate, window length, preprocessing, signal-to-noise ratio, embedding parameters, and pole-retention criteria. The strongest evidence therefore comes from within-dataset contrasts, convergence across independent estimator families, reproducibility of sleep-related dimensional downshifting across individuals, and cross-species reproduction in mouse sleep. The public synthetic component of the Aicumene EEG-BCI Sleep–Wake Dataset provides an additional construct-validity and pipeline-reproducibility test, but should not be interpreted as an independent biological replication. The coma descriptors were derived from relatively short recordings and show only modest single-recording reliability, which likely attenuates individual-level separation. The meditation dataset is small, and expertise effects may reflect arousal, breathing, strategy, or other behavioral differences. Most importantly, the organized-suppression signature is well supported in intact reversible states but remains only a candidate dynamical phenotype in coma. The present work is therefore not a clinical decision tool; it defines a mechanistic framework and a falsifiable

Aicumene:2026.042v2 [q-bio.NC] October 24, 2026

prospective target.

In summary, the decisive property of a quiet brain may be not how suppressed it is, but whether its dynamics remain organized and controllable. Intact brains regulate oscillator dimensionality, expanding their dynamical repertoire for engagement and contracting it for sleep, anesthesia, recovery, or efficient control. Severe injury can disrupt this regulation and produce pathological mode proliferation instead of organized dimensional contraction. The resulting clinical hypothesis is specific: *preserved capacity for organized dimensional downshifting may mark residual dynamical control that conventional static EEG descriptors do not capture*. Retrospective outcome labels cannot determine whether that capacity corresponds to biological recoverability. The decisive test is a prospective, withdrawal-blind or withdrawal-delayed study of dimensional state-transition capacity in post-anoxic coma.

Methods

Datasets and cohort selection

We analyzed public brain time-series datasets spanning intact wakefulness, reversible loss of consciousness, trained waking control, and post-anoxic coma. These included Sleep-EDF Expanded human polysomnography, OpenNeuro ds006366 mouse sleep, OpenNeuro ds005620 propofol anesthesia, OpenNeuro ds001787 meditation, and PhysioNet I-CARE post-cardiac-arrest coma. An independent controlled-access cohort of Aicumene wearable-EEG recordings was used for biological validation of the sleep-stage ordering; the public synthetic component of the Aicumene EEG-BCI Sleep–Wake Dataset was used separately for reproducibility and construct-validity analyses. For I-CARE, analyses were restricted to the public training partition with accessible EEG and outcome labels; 575 patients and 826 recordings at 24–72 h were used for oscillator-dimensionality and fusion analyses, and 500 patients with a common 19-channel montage were used for discriminative-subspace analysis.

Aicumene:2026.042v2 [q-bio.NC] October 24, 2026

Preprocessing and windowing

Recordings were restricted to EEG channels, band-pass filtered to 0.5–40 Hz, resampled where needed, segmented into non-overlapping windows, and analyzed with light uniform preprocessing. Flat or non-finite channels and windows with near-zero variance were excluded. Window-level descriptors were aggregated to subject-, recording-, or patient-level medians before statistical comparison to avoid inflated significance from correlated windows.

BOID and dynamical-organization descriptors

The generating model is the Bernadotte oscillator model of multichannel brain signals, a structured finite-mode model in which each channel is a superposition of damped sinusoids with shared poles (Supplementary Materials) [3, 8, 7]. For each multichannel window, we formed a block-Hankel delay embedding and estimated the signal-subspace rank using a multichannel singular-spectrum-analysis front end followed by ESPRIT pole extraction. BOID was defined as the number of recovered positive-frequency oscillatory modes in the 1–40 Hz range. We paired BOID with descriptors of dynamical organization, including estimator dispersion across independent intrinsic-dimension estimators, spectral entropy, Hankel participation ratio, mode-frequency entropy, and persistent-homology summaries of reconstructed trajectories.

Coma outcome analysis and subspace classifier

For I-CARE, Good outcome was defined as CPC 1–2 and Poor outcome as CPC 3–5. We tested a pre-specified pathological mode-proliferation index combining high mode count, high-frequency poles, burst intermittency, and mode-frequency entropy. We also evaluated a Hankel/MSSA discriminative-subspace classifier in which each recording was represented by its leading signal-subspace projector and scored in the low-dimensional class-separation subspace defined by $\Delta = P_{\text{Good}} - P_{\text{Poor}}$. All coma associations were interpreted as predicting observed, withdrawal-confounded outcome rather than biological recoverability.

Aicumene:2026.042v2 [q-bio.NC] October 24, 2026

Statistical analysis

Across-state comparisons used subject- or patient-level aggregated descriptors. Multistate comparisons used Kruskal–Wallis tests; paired two-condition contrasts used Wilcoxon signed-rank tests; two-group contrasts used Mann–Whitney tests; and classification performance was assessed using patient- or subject-grouped cross-validation. For the fused coma pipeline, feature families were evaluated under outcome-stratified, patient-grouped five-fold cross-validation, with significance assessed by patient-level permutation tests where stated. Additional mathematical details, reliability analyses, and robustness checks are provided in the Supplementary Materials.

Aicumene:2026.042v2 [q-bio.NC] October 24, 2026

References

[1] Brown, E. N., Lydic, R. & Schiff, N. D. General anesthesia, sleep, and coma. *New England Journal of Medicine* **363**, 2638–2650 (2010). https://doi.org/10.1056/NEJMra0808281.

[2] Adam, E. et al. Modulatory dynamics mark the transition between anesthetic states of unconsciousness. *Proceedings of the National Academy of Sciences* **120**, e2300058120 (2023). https://doi.org/10.1073/pnas.2300058120.

[3] Bernadotte, A. Topology-driven classification of time series. Preprint *bioRxiv* (2026). https://doi.org/10.64898/2026.04.25.720787.

[4] Bernadotte, A. & Menshikov, I. Brain oscillator intrinsic dimension marks consciousness, recovery mode and failed downshifting in coma. Aicumene preprint (2026). Available at: https://research.aicumene.com/papers/boid-coma/. https://doi.org/10.13140/RG.2.2.31610.25288.

[5] Bernadotte, A. & Buchstaber, V. Method for evaluating the number of signal sources and application to non-invasive brain-computer interface. Preprint *arXiv* arXiv:2410.11844 (2024). https://doi.org/10.48550/arXiv.2410.11844.

[6] Bernadotte, A. & Menshikov, I. Multichannel singular spectrum analysis for estimating oscillatory sources and localizing attenuating oscillations. Aicumene preprint (2026). Available at: https://research.aicumene.com/papers/MSSA/. https://doi.org/10.13140/RG.2.2.26719.01442. Version 2 (November 11, 2026) is divided into two papers: *Multichannel Singular Spectrum Analysis: Counting Oscillatory Modes and Recovering Their Spatial Loadings*, Aicumene Preprint 2026.044v2, SSRN 7693202, doi:10.2139/ssrn.7693202, and *From Oscillatory Modes to Source Geometry: Identifiability and Localization in Multichannel Time Series*, Aicumene Preprint 2026.058v1, SSRN 7716058, doi:10.2139/ssrn.7716058.

[7] Menshikov, I., Elfimov, N. & Bernadotte, A. A lightweight Hankel-embedded pipeline for real-time EEG filtering and classification. In *Proceedings of the 12th International Conference*

Aicumene:2026.042v2 [q-bio.NC] October 24, 2026

on Automation, Robotics and Applications (ICARA 2026), 589–593 (IEEE, 2026). https://doi.org/10.1109/ICARA69401.2026.11480292.

[8] Bernadotte, A. Estimating the number of sources in EEG with Hankel embedding for brain-computer interface. In *Proceedings of the 12th International Conference on Automation, Robotics and Applications (ICARA 2026)*, 621–626 (IEEE, 2026). https://doi.org/10.1109/ICARA69401.2026.11480398.

[9] Buchstaber, V. M. Time series analysis and Grassmannians. *American Mathematical Society Translations, Series 2* **162**, 1–17 (1994). https://doi.org/10.1090/trans2/162/01.

[10] Roy, R. & Kailath, T. ESPRIT: Estimation of signal parameters via rotational invariance techniques. *IEEE Transactions on Acoustics, Speech, and Signal Processing* **37**, 984–995 (1989). https://doi.org/10.1109/29.32276.

[11] Kuramoto, Y. *Chemical Oscillations, Waves, and Turbulence* (Springer, 1984).

[12] Acebrón, J. A., Bonilla, L. L., Pérez Vicente, C. J., Ritort, F. & Spigler, R. The Kuramoto model: A simple paradigm for synchronization phenomena. *Reviews of Modern Physics* **77**, 137–185 (2005). https://doi.org/10.1103/RevModPhys.77.137.

[13] Izhikevich, E. M. Simple model of spiking neurons. *IEEE Transactions on Neural Networks* **14**, 1569–1572 (2003). https://doi.org/10.1109/TNN.2003.820440.

[14] Izhikevich, E. M. *Dynamical Systems in Neuroscience: The Geometry of Excitability and Bursting* (MIT Press, 2007).

[15] Rissanen, J. Modeling by shortest data description. *Automatica* **14**, 465–471 (1978). https://doi.org/10.1016/0005-1098(78)90005-5.

[16] Grünwald, P. D. *The Minimum Description Length Principle* (MIT Press, 2007).

[17] Kemp, B. et al. Analysis of a sleep-dependent neuronal feedback loop: The slow-wave micro-continuity of the EEG. *IEEE Transactions on Biomedical Engineering* **47**, 1185–1194 (2000). https://doi.org/10.1109/10.867928.

Aicumene:2026.042v2 [q-bio.NC] October 24, 2026

[18] Levina, E. & Bickel, P. J. Maximum likelihood estimation of intrinsic dimension. In *Advances in Neural Information Processing Systems* **17**, 777–784 (2005).

[19] Facco, E., d'Errico, M., Rodriguez, A. & Laio, A. Estimating the intrinsic dimension of datasets by a minimal neighborhood information. *Scientific Reports* **7**, 12140 (2017). https://doi.org/10.1038/s41598-017-11873-y.

[20] Brito, M. R., Quiroz, A. J. & Yukich, J. E. Intrinsic dimension identification via graph-theoretic methods. *Journal of Multivariate Analysis* **116**, 263–277 (2013). https://doi.org/10.1016/j.jmva.2012.12.007.

[21] Camastra, F. & Staiano, A. Intrinsic dimension estimation: Advances and open problems. *Information Sciences* **328**, 26–41 (2016). https://doi.org/10.1016/j.ins.2015.08.029.

[22] Rose, L. et al. Probability estimation of narcolepsy type 1 in DTA mice using unlabeled EEG and EMG data. *SLEEP Advances* **6**, zpaf025 (2025). https://doi.org/10.1093/sleepadvances/zpaf025.

[23] Rose, L. et al. Mouse Sleep Staging Validation dataset (MSSV). *NEMAR* dataset, version 1.0.0 (2026). https://doi.org/10.82901/nemar.on006366.

[24] Bajwa, I. J. et al. A repeated awakening study exploring the capacity of complexity measures to capture dreaming during propofol sedation. *Scientific Reports* **15**, 32746 (2025). https://doi.org/10.1038/s41598-025-12695-z.

[25] Delorme, A. & Brandmeyer, T. EEG meditation study. *OpenNeuro* dataset ds001787, version 1.0.2. https://doi.org/10.18112/openneuro.ds001787.v1.0.2.

[26] Amorim, E. et al. The International Cardiac Arrest Research Consortium electroencephalography database. *Critical Care Medicine* **51**, 1802–1811 (2023). https://doi.org/10.1097/CCM.0000000000006074.

[27] Amorim, E. et al. I-CARE: International Cardiac Arrest REsearch consortium database, version 2.1. *PhysioNet* (2023). https://doi.org/10.13026/m33r-bj81.

Aicumene:2026.042v2 [q-bio.NC] October 24, 2026

[28] Sandroni, C. et al. Prediction of poor neurological outcome in comatose survivors of cardiac arrest: A systematic review. *Intensive Care Medicine* **46**, 1803–1851 (2020). https://doi.org/10.1007/s00134-020-06198-w.

[29] Elmer, J. et al. Association of early withdrawal of life-sustaining therapy for perceived neurological prognosis with mortality after cardiac arrest. *Resuscitation* **102**, 127–135 (2016). https://doi.org/10.1016/j.resuscitation.2016.01.016.

[30] Reyna, M. A. et al. Predicting neurological recovery from coma after cardiac arrest: The George B. Moody PhysioNet Challenge 2023. *Computing in Cardiology* **50** (2023). https://doi.org/10.22489/CinC.2023.019.

[31] Zabihi, M., Chaman Zar, A., Grover, P. & Rosenthal, E. S. Hyperensemble learning from multimodal biosignals to robustly predict functional outcome after cardiac arrest. *Computing in Cardiology* **50** (2023). https://doi.org/10.22489/CinC.2023.142.

[32] Tjepkema-Cloostermans, M. C. et al. Outcome prediction in postanoxic coma with deep learning. *Critical Care Medicine* **47**, 1424–1432 (2019). https://doi.org/10.1097/CCM.0000000000003854.

[33] Povinelli, R. J. & Dupont, R. A dynamical systems approach to predicting patient outcome after cardiac arrest. *arXiv* arXiv:2405.08827 (2024).

[34] Dionisio, J. et al. Is attention all you need for EEG to predict neurological outcomes in cardiac arrest? In *Proceedings of the IEEE EMBS International Conference on Biomedical and Health Informatics* (IEEE, 2024). https://doi.org/10.1109/BHI62660.2024.10913569.

[35] Zheng, W.-L. et al. Predicting neurological outcome from electroencephalogram dynamics in comatose patients after cardiac arrest with deep learning. *IEEE Transactions on Biomedical Engineering* **69**, 1813–1825 (2022). https://doi.org/10.1109/TBME.2021.3139007.

[36] Nesaragi, N., Qadir, A., Halvorsen, P. & Balasingham, I. Biaxialformer: Leveraging channel independence and inter-channel correlations in EEG signal decoding for predicting neurological outcomes. *arXiv* arXiv:2507.02879 (2025).

Aicumene:2026.042v2 [q-bio.NC] October 24, 2026

[37] Niu, Y. et al. Explainable machine learning model based on EEG, ECG, and clinical features for predicting neurological outcomes in cardiac arrest patients. *Scientific Reports* **15**, 11498 (2025). https://doi.org/10.1038/s41598-025-93579-0.

[38] Rohr, M. et al. Transformer network with time prior for predicting clinical outcome from EEG of cardiac arrest patients. *Computing in Cardiology* **50** (2023). https://doi.org/10.22489/CinC.2023.173.

[39] Grassberger, P. & Procaccia, I. Characterization of strange attractors. *Physical Review Letters* **50**, 346–349 (1983). https://doi.org/10.1103/PhysRevLett.50.346.

[40] Bernadotte, A. & Gromov, V. A. What is strong AI? Intrinsic structural criteria for strong intelligence based on dimensionality and topology. Aicumene preprint 2025.043v2 (2026). Available at: https://research.aicumene.com/papers/StrongAI/.

[41] Bernadotte, A. & Menshikov, I. From brain dynamics to strong artificial intelligence: learning creates functional regime switching. Oscillatory dimensionality, modes, stores, and clocks in trained neural systems. Aicumene preprint 2026.045v1 (October 2026). Available at: https://research.aicumene.com/papers/ACT-BOID/. https://doi.org/10.13140/RG.2.2.22357.59364.

[42] Gromov, V. A., Borodin, N. S. & Yerbolova, A. S. A language and its dimensions: intrinsic dimensions of language fractal structures. *Complexity* **2024**, 8863360 (2024). doi:10.1155/2024/8863360.

[43] Tulchinskii, E. et al. Intrinsic dimension estimation for robust detection of AI-generated texts. *Advances in Neural Information Processing Systems* **36** (2023). arXiv:2306.04723.

[44] Hamilton, J. D. A new approach to the economic analysis of nonstationary time series and the business cycle. *Econometrica* **57**, 357–384 (1989). doi:10.2307/1912559.

[45] Scheinkman, J. A. & LeBaron, B. Nonlinear dynamics and stock returns. *Journal of Business* **62**, 311–337 (1989). doi:10.1086/296465.

Aicumene:2026.042v2 [q-bio.NC] October 24, 2026

[46] Hsieh, D. A. Chaos and nonlinear dynamics: application to financial markets. *Journal of Finance* **46**, 1839–1877 (1991). doi:10.1111/j.1540-6261.1991.tb04646.x.

[47] Brock, W. A., Scheinkman, J. A., Dechert, W. D. & LeBaron, B. A test for independence based on the correlation dimension. *Econometric Reviews* **15**, 197–235 (1996). doi:10.1080/07474939608800353.

[48] Hassani, H., Heravi, S. & Zhigljavsky, A. Forecasting European industrial production with singular spectrum analysis. *International Journal of Forecasting* **25**, 103–118 (2009). doi:10.1016/j.ijforecast.2008.09.007.

[49] Golyandina, N., Nekrutkin, V. & Zhigljavsky, A. *Analysis of Time Series Structure: SSA and Related Techniques* (Chapman & Hall/CRC, 2001). doi:10.1201/9781420035841.

Acknowledgments

We thank the investigators and participants who made the public datasets used in this study available through PhysioNet and OpenNeuro.

Funding: The research was self-funded by the authors; no external funding was received.

Author contributions: A.B. conceived the study, developed the BOID and MSSA framework, designed the analyses, interpreted the results, contributed to computational implementation, and wrote the manuscript. I.M. contributed to computational implementation, developed the MSSA framework, analysis workflow, and wrote the manuscript.

Competing interests: The authors are co-founders of Aicumene and hold intellectual-property interests related to brain-signal processing, neurofeedback, and brain–computer interface technologies.

Data, code and materials availability: The publicly available datasets analyzed in this study are accessible through PhysioNet and OpenNeuro: the Sleep-EDF Expanded and I-CARE databases

Aicumene:2026.042v2 [q-bio.NC] October 24, 2026

(PhysioNet), and datasets ds006366, ds005620, and ds001787 (OpenNeuro). Accession identifiers and source references are provided in the Methods and Supplementary Information.

The Aicumene wearable-EEG recordings analyzed in this study comprise de-identified human electrophysiological recordings with sleep-stage annotations acquired using Aicumene BCI devices. These recordings are not publicly released. De-identified data may be made available to qualified researchers for legitimate non-commercial scientific research under controlled access. Requests should be directed to the corresponding author at bernadotte@aicumene.com and are subject to applicable participant-consent, ethical, privacy, data-protection, and data-use-agreement requirements.

The companion Aicumene EEG-BCI Sleep–Wake Dataset comprises a public synthetic benchmark and a controlled-access real-recording component. The public component consists of a synthetic sleep-EEG benchmark generated from a population model fitted to Sleep-EDF Expanded (Sleep Cassette) and used for reproducible validation of the analysis workflow. It is archived on Zenodo (DOI: 10.5281/zenodo.22923070) and documented in the companion repository at https://github.com/aicumene/aicumene-eeg-bci-sleep-wake-dataset. These recordings are synthetic surrogates and contain no real-subject signals. The controlled-access component consists of the de-identified Aicumene-device recordings described above.

Processed feature tables supporting the main figures and statistical analyses are available through Aicumene research resources at https://data.aicumene.com/, as described in the repository documentation.

Code required to reproduce the analyses is distributed across two repositories. The generic block-Hankel, multichannel singular spectrum analysis (MSSA), signal-subspace, and rank-estimation core is maintained at https://github.com/aicumene/MSSA. The Brain Oscillator Intrinsic Dimension (BOID) estimator, together with the intrinsic-dimension, topological, discriminative-subspace, and statistical analyses, is maintained at https://github.com/aicumene/BOID. The BOID package depends on the MSSA core rather than duplicating it, thereby maintaining a single canonical MSSA implementation and a single canonical BOID implementation across the public datasets, the synthetic benchmark, and the controlled-access Aicumene recordings.

Aicumene:2026.042v2 [q-bio.NC] October 24, 2026

Version history: Version 1 of this preprint (Aicumene:2026.042v1, July 2026, https://doi.org/10.13140/RG.2.2.31610.25288) reported the same datasets and cohort. Version 2 (October 24, 2026) aligns the results, figures, and interpretation with the manuscript under peer review, in particular the analysis of coma as withdrawal-confounded observed outcome, and adds the section *Beyond the brain*. The journal version carries the title "Brain states are organized by regulated oscillator dimensionality".

Supplementary materials

Materials and Methods

Supplementary Text

Figs. S1 to S3

Tables S1 and S2

Aicumene:2026.042v2 [q-bio.NC] October 24, 2026

Supplementary Materials for

Brain Oscillator Intrinsic Dimension marks consciousness, recovery mode, and failed downshifting in coma

Alexandra Bernadotte*, Ivan Menshikov

This PDF file includes:

Materials and Methods

Supplementary Text

Figures S1 to S3

Tables S1 and S2

Brain time-series datasets

We analyzed open brain time-series datasets that together span the range of conscious states, from alert wakefulness through graded loss of consciousness to the injured brain after cardiac arrest (Table S1). These comprised whole-night human polysomnography with expert sleep-stage annotations (Sleep-EDF Expanded), polysomnographic mouse sleep providing a supporting cross-species analysis (OpenNeuro ds006366), propofol anesthesia with repeated behavioral awakenings that dissociate the presence and absence of experience (OpenNeuro ds005620), expert-versus-novice focused-attention meditation (OpenNeuro ds001787), and continuous EEG from comatose survivors of cardiac arrest dichotomized by neurological outcome (PhysioNet I-CARE). The goal was not to build a single diagnostic model, but to test whether intrinsic dimension behaves as a general geometric marker of brain-state regime across physiologically and pathologically distinct routes to altered consciousness. Because sleep-stage labels in the mouse dataset were encoded numerically and not fully documented, mouse sleep was used as a supporting cross-species analysis rather than as a primary test of the theory; the stage assignment was based on delta/theta physiology as described in the main text.

Aicumene:2026.042v2 [q-bio.NC] October 24, 2026

Table S1: Open brain time-series datasets spanning the range of conscious states, from intact wakefulness through reversible loss of consciousness to post-anoxic coma.

Dataset	Modality	Conditions
Sleep-EDF Expanded [17]	Human PSG/EEG	Wake / N1 / N2 / N3 / REM (n = 10 subjects)
OpenNeuro ds006366 [23, 22]	Mouse PSG/EEG	Wake / NREM / REM (cross-species replication)
OpenNeuro ds005620 [24]	EEG	Awake vs. propofol-sedated (repeated awakenings)
OpenNeuro ds001787 [25]	EEG	Expert meditators (n = 12) Novice meditators (n = 12)
PhysioNet I-CARE [26, 27]	Continuous EEG	Comatose post-cardiac-arrest; Good vs. Poor outcome (n = 575, 24–72 h)
Aicumene wearable-EEG recordings	Human PSG/EEG	Wake / N1 / N2 / N3 / REM (n = 40 subjects)
Aicumene EEG-BCI Sleep–Wake synthetic benchmark	Human PSG/EEG	Wake / N1 / N2 / N3 / REM (n = 45 subjects)

Aicumene:2026.042v2 [q-bio.NC] October 24, 2026

I-CARE Dataset and cohort selection We analyzed the International Cardiac Arrest Research consortium (I-CARE) database, released for the George B. Moody PhysioNet/Computing-in-Cardiology Challenge 2023 [27, 30]: continuous EEG with routine clinical variables from 1020 comatose survivors of cardiac arrest across seven hospitals in the USA and Europe, dichotomized at 3–6 months into Good (Cerebral Performance Category, CPC, 1–2) versus Poor (CPC 3–5) neurological outcome. Only the public training partition ($\sim 60\%$ of patients) is released; the validation (10%) and test (30%) partitions are permanently sequestered, with one hospital held out entirely to the test set. All analyses were therefore restricted to the public training partition and evaluated by leakage-free, patient-grouped cross-validation; we did not access the hidden test set, so our internal cross-validated AUROC is not directly comparable to the Challenge's hidden-test operating-point metric.

Inclusion criteria. (i) adult comatose cardiac-arrest patient in the public I-CARE training release; (ii) a defined outcome label (Good or Poor); (iii) at least one EEG recording containing a finite, non-flat segment within the first 72 h after return of spontaneous circulation (24 h for the early-window subspace analysis). No manual selection of artifact-free epochs was performed.

Exclusion criteria. (i) patients present only in the sequestered validation/test partitions (inaccessible); (ii) records that could not be retrieved or decoded, or that contained no usable EEG segment in the target window; (iii) *for the subspace-geometry classifier only*, patients lacking the complete 19-channel 10–20 montage, because the method compares signal subspaces within a common ambient space—patients recorded with additional channels were retained (the canonical 19 forming a subset), whereas those missing any canonical channel were excluded.

Resulting cohorts. Applying these criteria to the retrieved records yielded 575 patients (217 Good / 358 Poor; 826 recordings at 24–72 h) for the oscillator-dimensionality battery and multimodal fusion, and 500 patients (195 Good / 305 Poor; one $\leq$ 24 h recording per patient) for the discriminative-subspace classifier. Both cohorts preserve the $\sim 60\%$ majority of poor outcomes seen in the full dataset, and no patient contributed to more than one cross-validation fold.

Aicumene:2026.042v2 [q-bio.NC] October 24, 2026

In-house Aicumene neurointerface validation dataset We additionally analyzed an independent in-house dataset acquired with the Aicumene non-invasive EEG neurointerface platform. The dataset included 40 participants with sleep-stage annotations spanning wakefulness, N1, N2, N3, and REM. The same preprocessing, Hankel-delay embedding, MSSA/ESPRIT oscillator extraction, and BOID estimation pipeline used for the public Sleep-EDF analysis was applied without retuning analysis parameters.

The Aicumene dataset reproduced the Sleep-EDF dimensionality ordering. Subject-level median BOID declined from wakefulness to N1, N2, and N3 slow-wave sleep (17, 12, 8, and 4 modes, respectively), with REM in an intermediate regime (10 modes; Kruskal–Wallis $H = 40.0$, $p = 4.3 \times 10^{-8}$). This independent validation supports the interpretation that sleep-related dimensional downshifting is not specific to Sleep-EDF, clinical polysomnography, or a particular public dataset, but generalizes to wearable EEG neurointerface recordings.

Brain time series representation

Let

$$\mathbf{X}_n = \big(x_1(t_n), \ldots, x_C(t_n)\big)^\top \in \mathbb{R}^C, \qquad n = 1, \ldots, N, \tag{S1}$$

denote a multichannel brain time series over C channels (electrodes or regions of interest). Recordings were segmented into non-overlapping analysis windows

$$W_s = \{\mathbf{X}_s, \ldots, \mathbf{X}_{s+T-1}\} \tag{S2}$$

of length T. Throughout the Methods, C denotes the number of channels, L the embedding length, Δ the delay in samples, m the number of resolved oscillatory modes, r_0 the ideal structured rank of a noiseless finite-mode signal, and $\widehat{r}$ the empirically estimated signal-subspace rank.

Hankel-delay embedding

For each multichannel window we formed delay vectors

$$Z_n = \left[\mathbf{X}_n^\top, \mathbf{X}_{n-\Delta}^\top, \ldots, \mathbf{X}_{n-(L-1)\Delta}^\top\right]^\top \in \mathbb{R}^{CL}. \tag{S3}$$

Their collection $\mathcal{T}_X = \{Z_n\}$ defines the reconstructed trajectory. Equivalently, the delay vectors are the columns of a multichannel block-Hankel trajectory matrix $H_X \in \mathbb{R}^{CL \times M}$, where M is the number

Aicumene:2026.042v2 [q-bio.NC] October 24, 2026

of valid delay vectors in the analysis window [9, 5, 3, 6, 7, 8]. All geometric and intrinsic-dimension analyses below act on this reconstructed trajectory or on its associated signal subspace. BOID is a specific oscillator-dimensionality read-out and is not identified with a generic intrinsic-dimension estimator.

Brain oscillator intrinsic dimension in the Bernadotte oscillator model (a structured finite-mode model)

We estimate the oscillator dimensionality of brain signals within the structured finite-mode framework introduced in Ref. [3] and extended to multichannel time series through multichannel singular spectrum analysis (MSSA) in Ref. [6]. The resulting framework is further specialized to neural recordings in Refs. [7, 8].

Our working model is that, within a sufficiently short analysis window, the structured component of a neural time series can be approximated by a finite superposition of dynamical modes. The scalar theory in Ref. [3] considers signals of the form

$$g(t) = \sum_{i=1}^{k_1} a_i e^{\alpha_i t} + \sum_{j=1}^{k_2} b_j \sin(\omega_j t + \phi_j) + \sum_{\ell=1}^{k_3} c_\ell e^{\lambda_\ell t} \sin(\nu_\ell t + \psi_\ell), \tag{S4}$$

where the first term represents real exponential modes, the second harmonic modes, and the third exponentially modulated oscillatory modes. For real, pairwise non-degenerate components, the associated delay-embedding trajectory K_g is contained in a linear subspace L,

$$K_g \subset L, \tag{S5}$$

whose dimension satisfies

$$\dim L \leq k_1 + 2k_2 + 2k_3. \tag{S6}$$

The component-to-dimension relation has a direct algebraic interpretation. A real exponential contributes one independent direction to the delay-embedding space. A harmonic component contributes the two-dimensional plane generated by its sine and cosine sequences, whereas an exponentially modulated oscillation is represented by the conjugate exponential pair

$$e^{(\lambda_\ell + i\nu_\ell)t}, \qquad e^{(\lambda_\ell - i\nu_\ell)t}, \tag{S7}$$

Aicumene:2026.042v2 [q-bio.NC] October 24, 2026

and therefore also contributes two independent directions. Because Hankel embedding is linear in the signal, the complete trajectory lies in the sum of the component subspaces. Under generic non-degeneracy and linear-independence conditions, the bound in Eq. (S6) is tight [3].

Defining the total number of oscillatory modes as

$$m_{\mathrm{osc}} = k_2 + k_3, \tag{S8}$$

the generic finite-component relation becomes

$$\dim L = k_1 + 2m_{\mathrm{osc}}, \tag{S9}$$

and hence

$$m_{\mathrm{osc}} = \frac{\dim L - k_1}{2}. \tag{S10}$$

Thus, in the ideal structured model, oscillator count is encoded in the dimension of the Hankel subspace. In the oscillation-only case ($k_1 = 0$), this reduces to $m_{\mathrm{osc}} = \dim L/2$; for a noiseless finite sequence, and subject to an adequate embedding window and non-degenerate mode parameters, the corresponding Hankel-rank relation is

$$r_0 = 2m_{\mathrm{osc}}. \tag{S11}$$

For multichannel neural recordings we use a shared-mode extension in which the temporal modes are common across channels but have channel-specific spatial loadings [6]. Pure harmonic and exponentially modulated oscillatory components are represented by one oscillator family by allowing the damping parameter to vanish:

$$\mathbf{X}(t) = \sum_{i=1}^{k_1} \mathbf{a}_i e^{\alpha_i t} + \sum_{j=1}^{m} \mathbf{b}_j e^{\beta_j t} \sin(\omega_j t + \varphi_j) + \boldsymbol{\varepsilon}(t), \tag{S12}$$

where $\mathbf{a}_i, \mathbf{b}_j \in \mathbb{R}^C$ are spatial loading patterns, α_i and β_j are growth or damping rates, ω_j is angular frequency, φ_j is phase, and $\boldsymbol{\varepsilon}(t)$ denotes noise and unresolved activity. Pure oscillations correspond to $\beta_j = 0$. Under the shared-mode assumption, spatial projection across channels does not create additional temporal poles; in the ideal noiseless, non-degenerate case the block-Hankel signal subspace therefore obeys

$$r_0 = \mathrm{rank}(H_X) = k_1 + 2m. \tag{S13}$$

Aicumene:2026.042v2 [q-bio.NC] October 24, 2026

For empirical recordings, however, BOID is not defined by halving an estimated matrix rank. The statistically supported multichannel signal subspace is first estimated with the MSSA procedure of Ref. [6], and its oscillatory content is then resolved by TLS-ESPRIT. If z_k denotes a recovered dynamical pole, its frequency for sampling rate F_s and shift Δ samples is

$$f_k = \frac{F_s}{2\pi\Delta} \arg(z_k). \tag{S14}$$

For real-valued signals, non-real poles occur as complex-conjugate pairs, so one positive-frequency pole represents one resolved physical oscillatory mode.

Brain oscillator intrinsic dimension (BOID) is therefore defined operationally as the number of resolved positive-frequency poles inside the analysis band,

$$\mathrm{BOID} = \#\left\{ z_k : f_{\min} \le \frac{F_s}{2\pi\Delta} \arg(z_k) \le f_{\max} \right\}. \tag{S15}$$

For the EEG analyses in this study, $f_{\min} = 1$ Hz and $f_{\max} = 40$ Hz.

In the ideal finite-mode limit, when all oscillatory modes are resolved and fall inside the analysis band,

$$\mathrm{BOID} = m = \frac{r_0 - k_1}{2}, \tag{S16}$$

and, when real-pole components are absent,

$$\mathrm{BOID} = \frac{r_0}{2}. \tag{S17}$$

In measured data, Eq. (S15), rather than the rank-halving relation, is the empirical definition used throughout the study. The MSSA signal-subspace estimator is treated here as an upstream method and is cited to the companion methodological work [6]; its derivation and recovery theory are not reproduced in the present paper.

Preprocessing and windowing

Across datasets we used deliberately light preprocessing so that within-dataset contrasts primarily reflected signal dynamics rather than analysis choices. Each recording was restricted to its EEG channels (the standard 10–20 montage where available; the single cortical EEG channel for the mouse data), band-pass filtered to 0.5–40 Hz, and resampled to 100 Hz (128 Hz for the mouse recordings, which were supplied at that rate). Oscillator and frequency descriptors were estimated

Aicumene:2026.042v2 [q-bio.NC] October 24, 2026

from non-overlapping 4-s windows. For sleep analyses, each 4-s BOID estimate was assigned by its midpoint to the corresponding manually scored 30-s sleep epoch, and the epoch-level BOID was the median of the assigned 4-s estimates; descriptors defined directly on the sleep epoch were computed on the 30-s window. Flat or non-finite channels were dropped, and windows containing non-finite samples or near-zero variance were skipped.

For inferential comparisons, window- or epoch-level descriptors were aggregated to one value per biological unit and condition (for example, subject × sleep stage) before group statistics were computed. We interpret within-dataset gradients rather than absolute BOID values across datasets, because absolute counts can depend on montage, sampling rate, window length, signal-to-noise ratio, and embedding parameters.

MSSA signal-subspace front-end and TLS-ESPRIT oscillator extraction

The oscillator descriptors—mode count, frequencies, damping rates, and mode amplitudes—were obtained from an MSSA signal-subspace front-end followed by TLS-ESPRIT pole extraction [6, 7, 8]. For each block-Hankel window, the MSSA implementation returns an empirically supported signal-subspace rank $\widehat{r}$ and a corresponding basis $\widehat{U}_s$. The rank-selection, noise-calibration, and recovery theory are part of the companion MSSA method and are described in Ref. [6]; they are not re-derived here.

TLS-ESPRIT was applied to $\widehat{U}_s$ using the shift invariance of the block-Hankel representation. If J_1 and J_2 select the two overlapping lag-shifted blocks,

$$U_1 = J_1\widehat{U}_s, \qquad U_2 = J_2\widehat{U}_s, \tag{S18}$$

and the shift operator satisfies

$$U_2 \simeq U_1\Phi, \tag{S19}$$

with Φ estimated by total least squares. Its eigenvalues $z_k \in \mathrm{eig}(\Phi)$ are the recovered dynamical poles. Their frequencies are obtained from Eq. (S14), and the pole magnitudes encode growth or damping.

Only resolved positive-frequency poles in the 1–40 Hz analysis band were counted toward BOID, according to Eq. (S15). The ideal relation BOID = $r_0/2$ is used only as a limiting theoretical relation; the empirical BOID value is the retained positive-frequency pole count.

Aicumene:2026.042v2 [q-bio.NC] October 24, 2026

From the retained modes we additionally computed the power-weighted mean and median oscillator frequency, the fraction of oscillatory power in predefined frequency bands, and the Shannon entropies of the mode-frequency and mode-power distributions. A surrogate-thresholded oscillatory-dimension descriptor d_{osc} was retained as a separate robustness measure and was not used to define BOID.

Discriminant validity: BOID versus signal complexity

Because BOID could be mistaken for a repackaging of established EEG complexity markers, we verified on synthetic signals with a *known* oscillator count that the two are not interchangeable. We generated signals with $m \in \{3, 12\}$ oscillators of random frequency (2–40 Hz), amplitude and phase, at two additive white-noise levels ($\sigma \in \{0.3, 1.5\}$ relative to unit-variance signal; 40 realizations per cell), and computed BOID (oscillator count from the ε-rank rule), normalized Lempel–Ziv complexity (LZ76 with median binarization), and spectral entropy. BOID tracked the ground-truth count (Pearson $r = 0.88$ with m) and preserved the mode-count ordering at both noise levels, whereas Lempel–Ziv complexity was governed mainly by noise ($r = 0.76$ with noise level versus $r = 0.50$ with m) and spectral entropy tracked m only weakly ($r = 0.25$). Diagnostically, a noisy three-oscillator signal scored *higher* on Lempel–Ziv complexity (1.02) than a clean twelve-oscillator signal (0.94)—an ordering BOID does not make. BOID therefore indexes the size of the oscillator repertoire (a rank), not sequence irregularity, and is a construct distinct from complexity-based markers of consciousness. On brain data, the corresponding partial-association test (BOID versus state and outcome after adjustment for Lempel–Ziv complexity and spectral entropy) is the natural confirmatory analysis; here its data-side counterpart is the coma feature-ablation, in which BOID and the intrinsic-dimension battery add information beyond spectral and burst-suppression descriptors (Fig. 4A).

Hankel spectral rank

For each Hankel matrix H_X, we computed the singular value decomposition

$$H_X = U\Sigma V^{\top}. \tag{S20}$$

Aicumene:2026.042v2 [q-bio.NC] October 24, 2026

From the singular values σ_i, we computed effective Hankel rank, energy rank, participation ratio, entropy rank, and stable rank:

$$d_{\mathrm{PR}} = \frac{\left(\sum_i \sigma_i^2\right)^2}{\sum_i \sigma_i^4}, \tag{S21}$$

$$d_{\mathrm{ent}} = \exp\left(-\sum_i p_i \log p_i\right), \qquad p_i = \frac{\sigma_i}{\sum_j \sigma_j}. \tag{S22}$$

These quantities provide linear estimates of the effective number of active Hankel components [5, 3, 7, 8].

Additional intrinsic dimension estimators

To avoid relying on a single estimator, we also computed nearest-neighbor and graph-based intrinsic dimension estimates, including the Levina–Bickel maximum likelihood estimator, TwoNN estimator, minimum-spanning-tree scaling estimators, and the Brito–Quiroz–Yukich MST-degree estimator [18, 19, 20, 21].

For each embedded point Z_i, let $T_j(Z_i)$ be the Euclidean distance to its j-th nearest neighbor. The local Levina–Bickel estimate for neighborhood size k is

$$\hat{d}_k(Z_i) = \left[\frac{1}{k-1}\sum_{j=1}^{k-1} \log \frac{T_k(Z_i)}{T_j(Z_i)}\right]^{-1}. \tag{S23}$$

The global estimate is obtained by averaging over embedded points and, where applicable, over a range of neighborhood sizes.

Agreement among estimators was interpreted as evidence for stable manifold-like structure. Disagreement was treated as a potential marker of nonstationarity, fragmentation, or departure from smooth low-dimensional dynamics.

Fractal estimators

As a check independent of the singular spectrum we additionally computed three established estimators. The Grassberger–Procaccia correlation dimension D_2 is the scaling exponent of the correlation integral $C(\epsilon) = \frac{2}{K(K-1)} \sum_{i<j} \mathbf{1}[\|Z_i - Z_j\| < \epsilon] \sim \epsilon^{D_2}$, estimated as the slope of $\log C$

Aicumene:2026.042v2 [q-bio.NC] October 24, 2026

versus $\log \epsilon$ over the lower-middle of the pairwise-distance distribution [39]. The false-nearest-neighbor embedding dimension is the smallest delay-embedding dimension at which the fraction of neighbors that separate on extending the embedding falls below a tolerance, computed per channel and averaged. The Higuchi fractal dimension is the slope of $\log L(k)$ versus $\log(1/k)$ for the curve length $L(k)$ of the series sub-sampled at lag k, again per channel and averaged. Because the correlation dimension acts on the multichannel delay embedding while the false-nearest-neighbor and Higuchi estimators act on the raw single-channel signals, their agreement with the spectral and graph estimators provides convergent evidence independent of the Hankel construction. The estimator-dispersion index Δ_{ID} is the inter-quartile range across the scalar estimators and is itself reported as a state descriptor.

Topological descriptors based on persistent homology

We computed persistent homology of reconstructed Hankel-delay trajectories using Vietoris–Rips filtrations. For each trajectory, we extracted H_0 and H_1 persistence diagrams, persistence entropy, the number of long-lived features, and vectorized topological summaries.

For a persistence diagram

$$D_q = \{(b_j, d_j)\}_j, \tag{S24}$$

we define lifetimes

$$\ell_j = d_j - b_j \tag{S25}$$

and persistence entropy

$$\mathrm{PersEntropy}(D_q) = -\sum_j p_j \log p_j, \qquad p_j = \frac{\ell_j}{\sum_k \ell_k}. \tag{S26}$$

The topological interpretation is direct: dominant oscillations produce loop-like structures; multiple oscillatory modes produce more complex cyclic structures; fragmentation or switching produces altered connected components and persistence patterns.

Aicumene:2026.042v2 [q-bio.NC] October 24, 2026

Grassmann discriminative-subspace classifier

Each multichannel recording X was represented by the r-dimensional signal subspace $U_r(X)$ of its block-Hankel trajectory. For each outcome class c, we formed the class mean projector

$$P_c = \left\langle U_i U_i^\top \right\rangle_{i \in c}, \tag{S27}$$

computed from the training recordings only. The class-separation operator was

$$\Delta = P_{\text{Good}} - P_{\text{Poor}}. \tag{S28}$$

Because Δ is symmetric, its eigenvectors provide orthogonal directions along which the two class-average projector representations differ. We retained the k eigenvectors with the largest absolute eigenvalues, defining a discriminative subspace W_k.

A query recording was scored by the signed energy of its Hankel signal subspace within these directions,

$$s(X) = \sum_{j=1}^{k} \lambda_j \left\| w_j^\top U_r(X) \right\|_F^2 = \mathrm{Tr}\big(U_r(X)^\top \Delta_k U_r(X)\big), \tag{S29}$$

where

$$\Delta_k = \sum_{j=1}^{k} \lambda_j w_j w_j^\top. \tag{S30}$$

The sign and magnitude of $s(X)$ quantify whether the recording projects more strongly onto Good- or Poor-associated discriminative directions. Taking k to the full rank of Δ recovers the score based on the complete class-separation operator; finite k restricts the read-out to its strongest discriminative directions.

Geometrically, each $U_r(X)$ is a point on the Grassmann manifold $\mathrm{Gr}(n, r)$ of r-planes in $\mathbb{R}^n$ ($n = CL$). This construction is motivated by the Grassmannian representation and subspace-separation framework introduced in Ref. [3]. That work also establishes perturbation stability of the recovered subspace under sufficiently small Hankel perturbations when a non-degenerate spectral gap is present. We therefore use the classifier as a low-dimensional geometric read-out of class differences, without invoking additional closed-form generalization or stability bounds.

Aicumene:2026.042v2 [q-bio.NC] October 24, 2026

Parameters and evaluation

For the discriminative-subspace classifier, the embedding window was fixed at $L = 12$. The signal-subspace rank r and discriminant dimension k were explored over a predefined grid. The classifier was evaluated on 500 comatose patients (195 Good / 305 Poor; one $\leq$ 24-h recording per patient) using patient-grouped cross-validation. Within every training fold, the class mean projectors and Δ were recomputed from training patients only, so no test-patient recording contributed to the discriminant operator. A patient-level label-permutation control collapsed performance to chance.

The best exploratory out-of-fold AUROC was 0.72 at $r = 12$ and $k \approx 3$–6. Because this value was selected as the maximum over the r, k grid using the same grouped cross-validation used to summarize performance, it should be regarded as mildly optimistic rather than as an unbiased tuned-performance estimate; strictly nested model selection would be required for that purpose. When added to the intrinsic-dimension battery and clinical-feature fusion, the discriminative-subspace score contributed an increment of 0.009 AUROC in the 30-seed repeated cross-validation analysis.

Algorithm S1. Grassmann discriminative-subspace classifier. The classifier proceeds as follows: (i) construct a block-Hankel embedding for each multichannel recording; (ii) compute the rank-r signal subspace from the lagged covariance; (iii) estimate class mean projectors P_A and P_B; (iv) form the class-separation operator $\Delta = P_A - P_B$; (v) retain the k eigenvectors with largest absolute eigenvalues; and (vi) classify a query recording by the signed energy of its signal subspace in these discriminative directions. Positive score components indicate projection onto A-characteristic directions and negative components onto B-characteristic directions.

Topology-driven classifier

For each window W_s, we constructed a feature vector

$$\Psi(W_s) = \left[\Psi_{\mathrm{ID}}, \Psi_{\mathrm{Hankel}}, \Psi_{\mathrm{PH}}, \Psi_{\mathrm{geom}}\right], \tag{S31}$$

where Ψ_{ID} collects the nearest-neighbor, graph and fractal intrinsic-dimension estimates, Ψ_{Hankel} the singular-spectrum descriptors, Ψ_{PH} the persistent-homology summaries, and Ψ_{geom} additional trajectory-geometry features (no raw band power or amplitudes enter Ψ). The classifier F is a

Aicumene:2026.042v2 [q-bio.NC] October 24, 2026

histogram gradient-boosting model with balanced class weights, evaluated under K-fold cross-validation *grouped by subject* (`GroupKFold`), so that no subject contributes windows to both the training and the test fold. We report balanced accuracy, macro-F_1, and (for binary contrasts) the ROC-AUC, with chance level $1/(\text{number of classes})$, together with permutation feature importance. For the I-CARE coma data the outcome label is per patient; all 575 patients with a usable 24- and/or 72-h recording were analyzed (the first 240 s of each). We tested whether *higher* oscillator dimensionality marks poor outcome in two ways. First, for each marker—the oscillator count, the mean oscillator frequency, and a pre-specified pathological mode-proliferation index, PMPI = z(n_modes) + z(hf-pole fraction) + z(burst intermittency) + z(mode-frequency entropy) (z-scored within each timepoint)—we report the discrimination AUC for predicting Poor outcome and a one-sided Mann–Whitney test. Second, a leakage-free, patient-grouped cross-validated logistic classifier (standardized features; `GroupKFold`, so no patient is split across folds) over the oscillator count, PMPI, and frequency descriptors was assessed by a patient-level label-permutation test (3000 permutations reassigning Good/Poor across patients; two-sided on $|\text{AUC} - 0.5|$).

For the fused prognostic pipeline, the per-recording features were grouped into four families: oscillator descriptors; the full intrinsic-dimension battery (Levina–Bickel MLE, TwoNN, correlation dimension, false-nearest-neighbors, MST-length, BQY-degree, persistent-homology H_1, effective and stable rank, Higuchi, and estimator dispersion); spectral and burst-suppression descriptors; and routine clinical variables. For each family and each union we trained both a histogram gradient-boosting classifier and an ℓ_2-regularized logistic model under outcome-stratified, patient-grouped five-fold cross-validation (`StratifiedGroupKFold`), reporting the better model per feature set scored by ROC-AUC, balanced accuracy, sensitivity at a false-positive rate $\leq 5\%$, and the Brier score. Significance was assessed by a 2000-fold patient-level permutation test on the winning model and on a three-modality out-of-fold stacked ensemble.

Dynamical organization axis and the coma test

Beyond the scalar dimension, we quantified how *organized* the low-dimensional dynamics were, using measures that are low when few coherent modes dominate and high when activity is fragmented: the estimator-dispersion index Δ_{ID} (disagreement among independent intrinsic-dimension estimators), spectral entropy, the participation ratio of the Hankel singular spectrum, mode-frequency

Aicumene:2026.042v2 [q-bio.NC] October 24, 2026

entropy, and the persistence structure of the delay embedding. The *organized-suppression signature* is the joint pattern of low BOID with low Δ_{ID}, low spectral entropy, and simple topology. We defined an organization axis from sleep as the direction separating the deepest recoverable-suppression state (N3, the organized pole) from wakefulness (the disorganized pole); in Sleep-EDF, Δ_{ID} ran $4.6 \rightarrow 1.1$ and spectral entropy $53 \rightarrow 22$ from wake to N3.

For the coma test we projected each I-CARE patient's per-recording median descriptors onto this axis (features standardized within the coma cohort) and asked whether more-organized patients had better outcome. On the powered cohort ($N = 494$) the combined organization score separated outcome only weakly (AUC ≈ 0.53, one-sided $p = 0.11$), with spectral entropy the strongest single component in the expected direction (higher in Poor, AUC 0.57, $p = 0.009$) but two components (stable rank, participation ratio) running counter to the sleep direction; direct fragmentation features in the hospital-tagged subset ($N = 32$) all trended the expected way but none reached significance. We explicitly did *not* convert this into a per-patient "recoverable-despite-Poor-label" flag: because the distributions overlap at AUC ≈ 0.53, roughly half of Poor-outcome patients fall above the Good median by chance alone, so such a count carries no information and is not reported.

Finally, the coma outcome is not an unconfounded ground truth. Because withdrawal-of-life-support decisions in post-anoxic coma are informed by the EEG, and a large fraction of poor outcomes follow withdrawal [29, 28], any EEG-derived marker is partly validated against decisions it helped make (a self-fulfilling prophecy). We therefore treat all coma associations as indexing current prognostic practice, not biological recoverability, and specify a prospective, withdrawal-blind or withdrawal-delayed design as the confirmatory test.

Statistical analysis and classification

All descriptor comparisons were performed on subject-level (or patient-level) medians, to avoid inflated significance from many correlated windows. Differences across more than two physiological states used the Kruskal–Wallis test across groups (the Friedman test for the within-subject sleep-stage design); within-subject two-condition contrasts (rest vs. task, awake vs. sedated) used the paired Wilcoxon signed-rank test; two-group contrasts (Good vs. Poor outcome, expert vs. novice) used the Mann–Whitney U test; and ordinal associations (with the CPC score) used the Spearman correlation. The primary endpoint is the direction of the BOID–outcome association in

Aicumene:2026.042v2 [q-bio.NC] October 24, 2026

post-anoxic coma (higher BOID with worse outcome); the intact-brain state contrasts (sleep, anesthesia, meditation) define the reference direction, and every other comparison—the full estimator battery, the descriptor families, and the fusion ablations—is secondary and exploratory. *P*-values are reported per descriptor; where a family of descriptors was screened this is stated explicitly, and secondary results are interpreted as hypothesis-generating rather than as independently confirmed effects. All cross-validation is grouped by subject or patient (no leakage), and significance of cross-validated decoding was, where stated, assessed by label permutation respecting the grouping. Analyses were implemented in Python with NumPy, SciPy, and scikit-learn (histogram gradient boosting; `GroupKFold` and `StratifiedGroupKFold` splitters), with persistent homology computed from Vietoris–Rips filtrations; the analysis code will be released as stated in the Data, code and materials availability section.

Comparison with coma-outcome prediction studies

To make the clinical-prognostic component interpretable in context, we compared our I-CARE analysis with representative published approaches using the I-CARE challenge dataset or closely related post-anoxic coma EEG cohorts (Table S2). The table is intended as contextual calibration rather than a leaderboard claim. Hidden-test challenge scores, internal cross-validation AUROC, leave-hospital-out validation, and external validation are not directly interchangeable. Our contribution is deliberately framed as a data-light and mechanistically interpretable geometric read-out of failed dimensional regulation, not as an optimized competition system.

Robustness and interpretation checks

The central claims are based on within-dataset contrasts and convergence across independent estimator families rather than on absolute BOID values. This is important because absolute oscillator counts can vary with montage, sampling rate, window length, preprocessing, signal-to-noise ratio, embedding parameters, and the pole-retention criterion. The analyses therefore followed five safeguards.

Subject- and patient-level aggregation. Window-level descriptors were reduced to subject-level or patient-level medians before statistical comparison. This prevents significance from being inflated

Aicumene:2026.042v2 [q-bio.NC] October 24, 2026

Table S2: Representative coma-outcome prediction studies using I-CARE or related post-anoxic coma EEG cohorts. Reported numbers are not directly comparable because input duration, modalities, artifact curation, validation protocol, hidden-test access, and operating-point tuning differ across studies. The table is provided to contextualize the prognostic component of the present work; the primary claim of this manuscript is a theory of regulated oscillator dimensionality.

Study	Input	Evaluation	AUROC	Sens.@5% FPR	Main caveat or distinction
Reyna et al. 2023 [30]	19-channel EEG, ECG, clinical variables	Hidden challenge test; one hospital held out	–	0.79	Official challenge overview and operating-point metric; AUROC not the main reported endpoint.
Zabihi et al. 2023 [31]	EEG, ECG, clinical variables	Hidden test plus internal validation	0.92	0.79	Hyperensemble optimized for the challenge metric; uses multimodal biosignals.
Tjepkema-Cloostermans et al. 2019 [32]	Continuous EEG after cardiac arrest	Deep-learning prognostication cohort	0.88–0.90	–	Strong deep-learning baseline, but not the same public I-CARE challenge evaluation.
Povinelli and Dupont 2024 [33]	EEG and clinical variables	Hidden-test challenge run	–	0.43	Dynamical-systems feature approach; large train-test discrepancy reported.
Dionisio et al. 2024 [34]	EEG power spectral density	Patient-wise, external, and hospital-wise analyses	0.82	–	Performance varied strongly by patient/hospital split and external validation.
Zheng et al. 2021 [35]	Long-duration multichannel EEG	Cross-validation on I-CARE consortium database	0.78	–	Uses the precursor consortium database rather than the frozen public challenge release.
Nesaragi et al. 2025 [36]	18-channel EEG	Leave-one-hospital-out cross-validation	0.77	0.52	Transformer-style EEG decoder; validation protocol differs from hidden challenge scoring.
Niu et al. 2025 [37]	qEEG, ECG, and clinical features	Small subset, internal splits	1.00	–	Reported perfect AUROC should be interpreted cautiously because it may indicate leakage or subset effects.
Rohr et al. 2023 [38]	Raw EEG with time prior	Cross-validation only	–	0.41	Reported score is not directly comparable to hidden-test challenge metrics.
This work	Approximately 4 min of 19-channel EEG plus routine clinical variables	Leakage-free patient-grouped cross-validation on public training partition	0.81	0.33	Data-light, no manual epoch curation; designed to test interpretable dimensional regulation rather than optimize leaderboard performance.

Aicumene:2026.042v2 [q-bio.NC] October 24, 2026

by many correlated windows and tests whether effects survive at the biological-unit level.

Estimator-family convergence. Human sleep was analyzed not only with BOID but also with fractal, nearest-neighbor, graph, Hankel-rank, and topological estimators. Scalar estimators from different mathematical families converged on the deep-sleep dimensional minimum, while topological descriptors separated REM by richer cyclic structure. This reduces the risk that the sleep-depth effect is an artifact of MSSA/ESPRIT alone.

Context-dependent interpretation. BOID was interpreted as a state-regime marker, not as a monotonic goodness score. Low dimensionality was treated as adaptive only in organized intact-brain contexts such as sleep, anesthesia, and expert meditation. High dimensionality was treated as adaptive only in engaged intact wakefulness, and as potentially pathological in injured post-anoxic coma. This context rule is central to the theory and prevents overinterpreting dimensionality as universally beneficial or harmful.

Clinical-prognostic caution. The I-CARE analysis was evaluated with patient-grouped cross-validation on the public training partition only. It was not treated as a stand-alone clinical decision tool and was not compared directly to hidden-test challenge scores. The coma analysis is used here primarily as a pathological stress test of dimensional regulation and secondarily as evidence that failed dimensional control carries prognostic information.

Estimator reliability and measurement attenuation. The coma BOID was computed from a short segment (≈ 4 min, i.e. ~ 60 windows of 4 s) per recording. Because a 4 s oscillator count is itself variable, a single short-segment BOID is a noisy estimate of a patient's central value: in our data the within-patient coefficient of variation was ≈ 0.4 (BOID could range from ~ 10 to ~ 65 within one patient over the recording), and a one-way random-effects decomposition gave an intraclass reliability of a single ≈ 4 min BOID of only ICC ≈ 0.4. Under a classical measurement-error interpretation, this level of within-patient variability is expected to attenuate between-group separation toward chance. An exploratory variance-components projection suggested that longer-recording aggregation could raise the bare-BOID discrimination from AUC ≈ 0.56 for the short-segment estimate toward approximately 0.60 under the assumptions of that model. This projection

Aicumene:2026.042v2 [q-bio.NC] October 24, 2026

is not treated as an empirical performance estimate or a formal upper bound; it is included only to quantify the likely scale of attenuation. The stronger prognostic signal in the present analysis arises from the multimodal fusion (AUC 0.81), rather than from a single short-segment BOID scalar. Full-recording aggregation and, critically, leave-one-hospital-out evaluation of the fusion model on the complete cohort are planned confirmatory analyses; the small subset with hospital labels available here (31 patients, 5 hospitals) is underpowered for a hospital-wise test and is reported only as a feasibility check.

Future validation should explicitly quantify sensitivity to window length, MSSA rank threshold, frequency range, montage, and artifact rejection strategy in prospective datasets. The present results should therefore be interpreted as evidence for a cross-state pattern of dimensional regulation, not as a fully calibrated clinical threshold.

Algorithmic summary

Algorithm S2. Intrinsic-dimension and topology-based analysis. For each subject, recordings were preprocessed and segmented into windows. Each window was converted to a Hankel-delay trajectory, decomposed by SVD, and summarized by rank-based, nearest-neighbor, graph, fractal, and topological descriptors. Descriptors were aggregated at subject or patient level, tested across brain states, and used in grouped cross-validation for classification analyses.

Aicumene:2026.042v2 [q-bio.NC] October 24, 2026

Dataset-level reproducibility checks

Within-subject reproducibility of sleep-related dimensional downshifting.

To verify that the sleep-depth effect was not driven by a single subject or by pooled-window statistics, we visualized whole-night BOID trajectories for each Sleep-EDF recording in the analyzed sample. In nearly all recordings, BOID was highest during wakefulness and lowest during N3 slow-wave sleep, with N1, N2, and REM occupying intermediate ranges. The running median followed the hypnogram over the night: dimensionality decreased during transitions into deeper NREM sleep and increased again during REM or wake transitions. This subject-level montage confirms that the reduction of BOID with sleep depth is reproducible across individuals and reflects a within-brain state transition from high-dimensional wakefulness to low-dimensional sleep recovery mode.

Individual-animal reproducibility of mouse sleep dimensional downshifting.

To verify that the mouse sleep effect was not driven by pooled epochs or a small number of animals, we visualized BOID trajectories separately for individual mice. Across recordings, non-REM sleep was associated with lower BOID than wakefulness, while REM generally occupied an intermediate or higher-dimensional regime. The within-animal boxplots reproduced the group-level ordering, and the time-resolved traces showed BOID decreasing during sustained non-REM periods and increasing during transitions back toward wakefulness or REM. These individual-animal trajectories support the conclusion that low-dimensional non-REM sleep is a conserved recovery-mode state across mammalian sleep.

Dataset-level reproducibility and construct-validity checks

As an additional construct-validity and reproducibility check, we analyzed the public synthetic component of the Aicumene EEG-BCI Sleep–Wake Dataset (DOI: 10.5281/zenodo.22923070). The benchmark consists of synthetic sleep-EEG surrogates generated from a population model fitted to Sleep-EDF Expanded and contains no real-subject signals. It was analyzed with the same BOID pipeline and the same sleep-stage convention used for the physiological sleep analyses.

The synthetic recordings reproduced the stage-dependent organization observed in the empirical

Aicumene:2026.042v2 [q-bio.NC] October 24, 2026

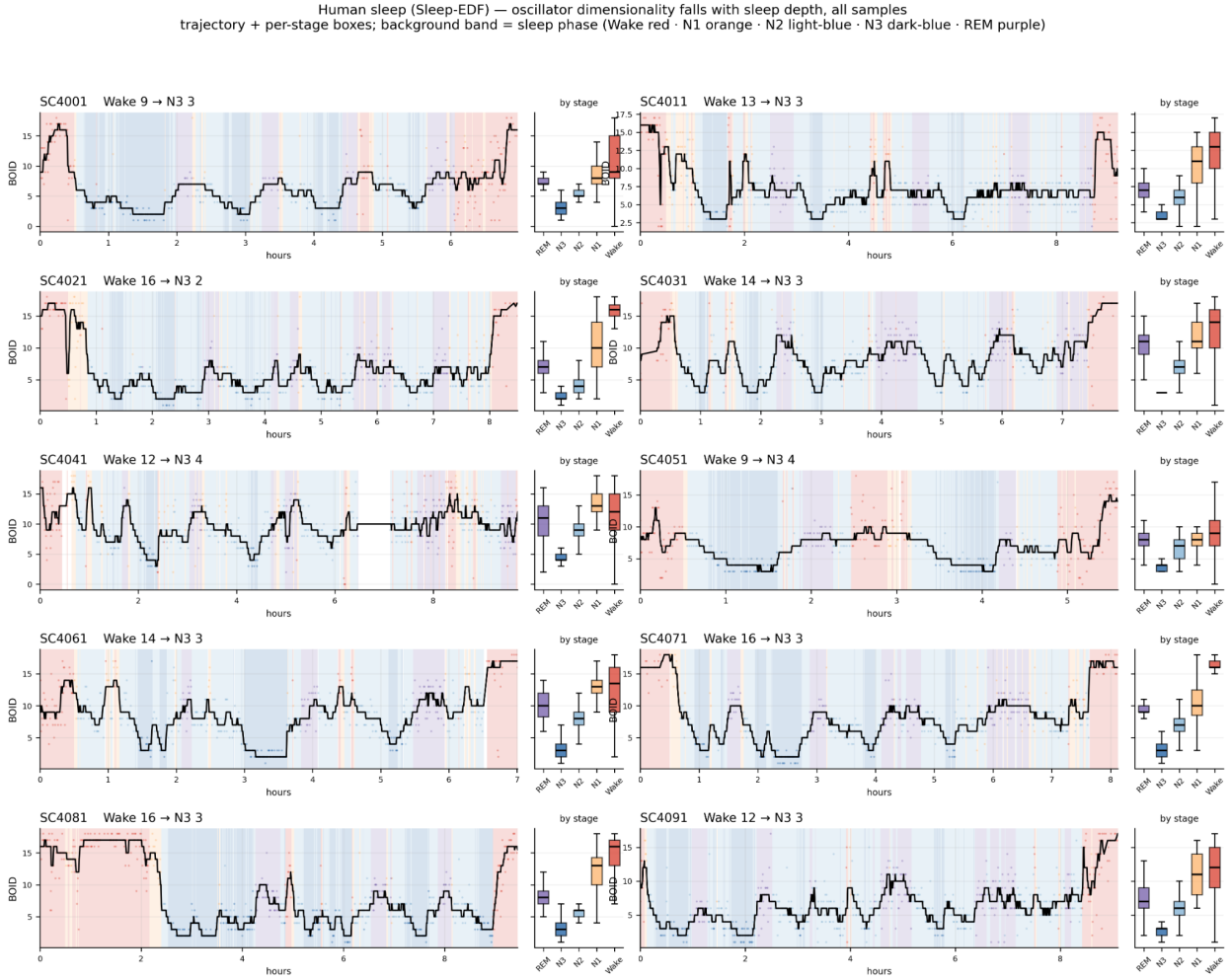

Figure S1: **Whole-night oscillator dimensionality trajectories across the Sleep-EDF human sleep sample.** Each panel shows one Sleep-EDF recording from the analyzed human sleep subset. The main trace in each panel is Brain oscillator intrinsic dimension (BOID) across the night. BOID was estimated in non-overlapping 4-s oscillator-analysis windows; each 4-s estimate was assigned by its midpoint to the corresponding manually scored 30-s sleep epoch, and the plotted epoch-level value is the median of the assigned 4-s estimates. Colored points indicate individual epochs; the black curve shows a running median. Background shading denotes manually scored sleep phase: Wake in red, N1 in orange, N2 in light blue, N3 in dark blue, and REM in purple. The small boxplot to the right of each trajectory summarizes BOID by sleep stage within the same recording. Across subjects, BOID is consistently highest during wakefulness, decreases during NREM sleep, and reaches its lowest values during N3 slow-wave sleep, with REM generally occupying an intermediate regime.

Aicumene:2026.042v2 [q-bio.NC] October 24, 2026

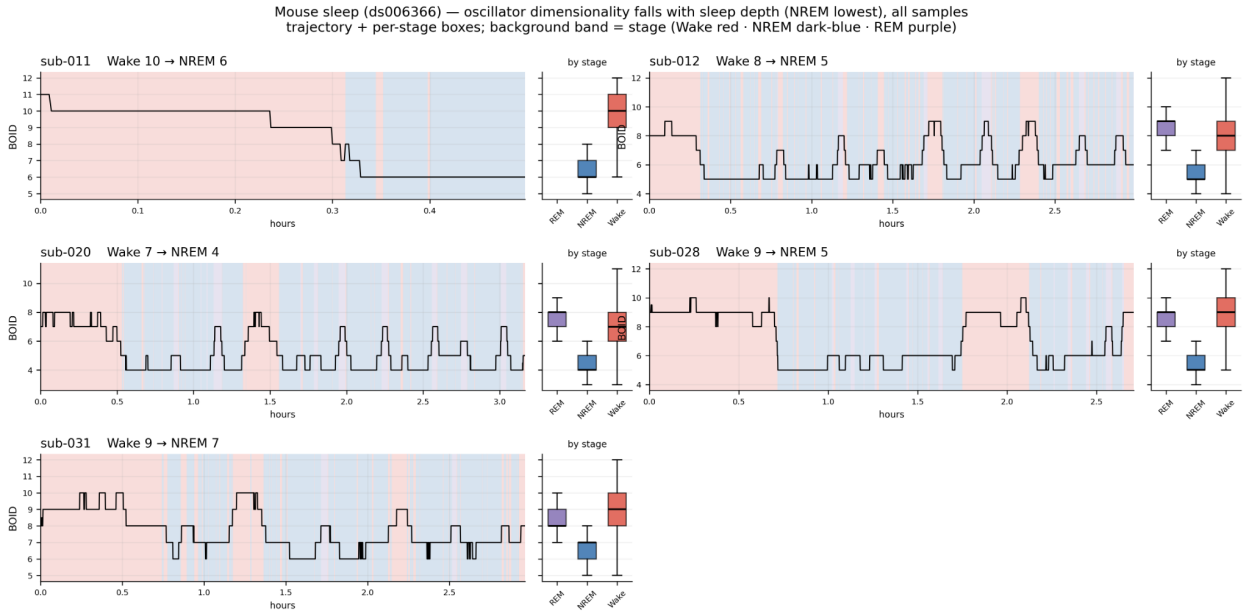

Figure S2: **Mouse sleep reproduces the low-dimensional non-REM state across individual animals.** Whole-recording BOID trajectories for representative mice from OpenNeuro ds006366. Each panel shows brain oscillator intrinsic dimension (BOID), computed as oscillator count across time, together with sleep-stage background shading. Wake is shown in red, non-REM sleep in dark blue, and REM in purple. The black step curve shows the BOID trajectory for each animal, and the adjacent boxplot summarizes BOID by sleep stage within the same recording. Across animals, BOID is consistently lower during non-REM sleep than during wakefulness, with REM generally occupying an intermediate or higher-dimensional regime. Panel titles report the within-animal Wake and non-REM medians, illustrating the repeated dimensional downshift from wakefulness into non-REM sleep. This montage shows that the mouse sleep effect is reproducible at the individual-animal level and is not driven by pooling epochs across animals.

Aicumene:2026.042v2 [q-bio.NC] October 24, 2026

human data. Across the illustrated recordings, oscillator dimensionality was consistently highest during wakefulness, decreased through lighter NREM sleep, and reached its minimum during N3 slow-wave sleep, with REM occupying an intermediate regime. In the eight synthetic recordings shown here, the median BOID during wakefulness ranged from approximately 14 to 17 modes, whereas the corresponding N3 medians ranged from approximately 2 to 4 modes. N1, N2, and REM occupied intermediate ranges.

Importantly, the reduction was visible not only in stage-pooled distributions but also in the temporal trajectories. BOID contracted during transitions into deep NREM sleep and expanded again during transitions toward REM or wakefulness. The synthetic benchmark therefore reproduces the characteristic dimensional downshifting observed in empirical sleep recordings at both the stage-distribution and within-recording trajectory levels.

Because these recordings are synthetic and their population structure was derived from Sleep-EDF, this analysis is not treated as an independent biological replication. Rather, it provides a controlled test that the BOID analysis recovers the expected ordering of dynamical regimes from surrogate signals with known sleep-state structure and does not require access to the original subject recordings.

State coherence of auxiliary signals in the synthetic benchmark

To verify that the synthetic sleep-state labels were embedded in a coherent multimodal physiological context rather than represented only in the EEG generator, we additionally inspected the auxiliary polysomnographic channels of the synthetic benchmark. These comprised the hypnogram, submental electromyography (EMG), electro-oculography (EOG), respiration, and body temperature.

The generated auxiliary signals exhibited stage-concordant structure across recordings. The clearest effect was observed in submental EMG: tonic muscle activity was high during wakefulness, generally decreased during NREM sleep, and reached its lowest level during REM periods, consistent with REM-associated muscle atonia. EOG activity varied across the night and remained temporally aligned with the simulated sleep-state sequence. Respiration retained a continuous oscillatory structure across stages, while body temperature varied smoothly over the night within a physiological range rather than changing abruptly at stage boundaries.

Aicumene:2026.042v2 [q-bio.NC] October 24, 2026

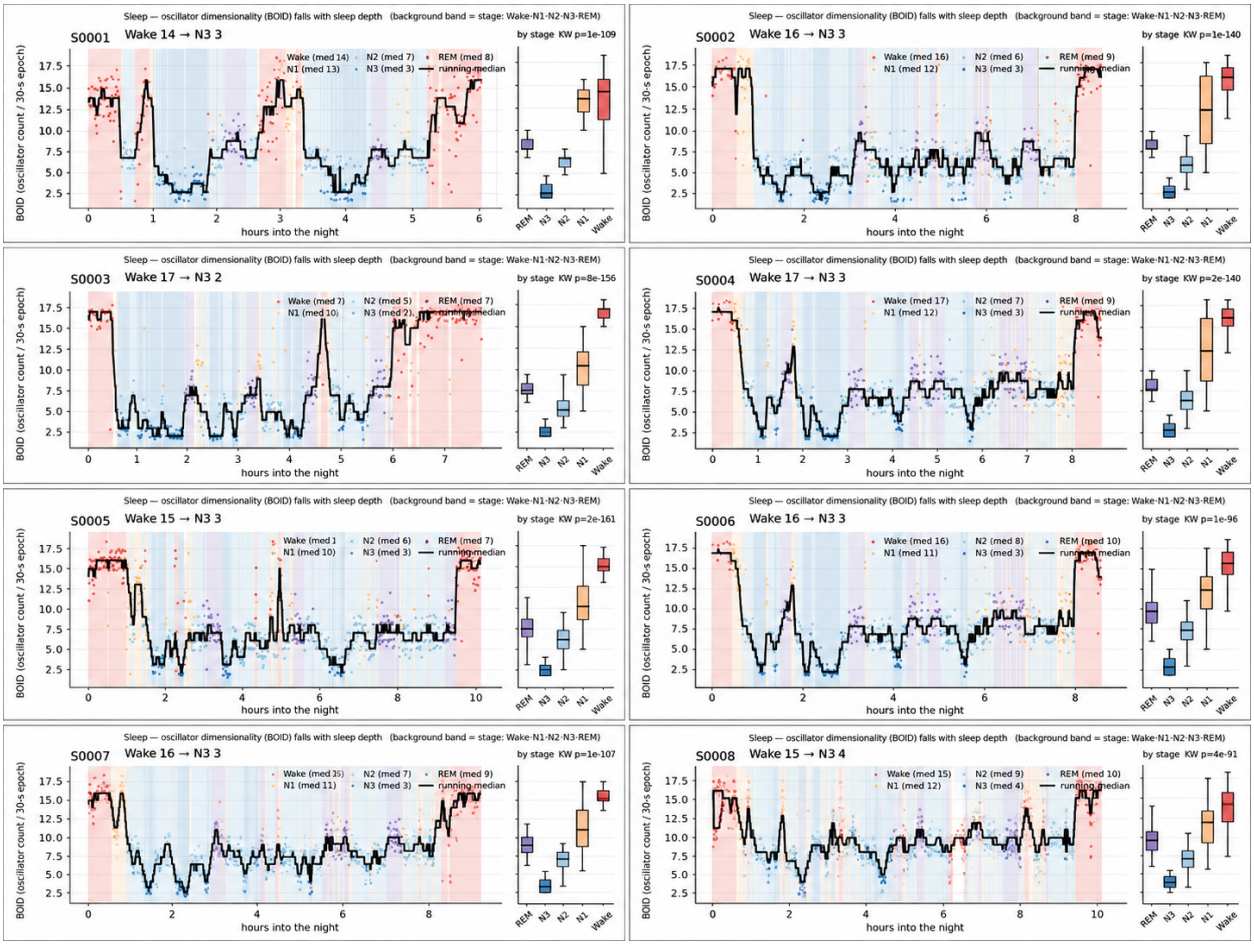

Figure S3: **Synthetic sleep-EEG benchmark reproduces stage-dependent oscillator dimensionality.** Representative recordings from the public synthetic component of the Aicumene EEG-BCI Sleep–Wake Dataset are shown individually. Each panel displays epoch-level brain oscillator intrinsic dimension (BOID) across a synthetic night. BOID estimates are summarized on the 30-s sleep-stage grid and coloured by concurrent stage: Wake (red), N1 (orange), N2 (light blue), N3 (dark blue), and REM (purple). The black trace is a running median and background shading denotes sleep stage. The boxplots at right summarize the BOID distribution within each stage of the same synthetic recording. Across recordings, wakefulness shows the largest oscillator repertoire, N3 the smallest, and N1, N2, and REM intermediate values. Kruskal–Wallis p values shown in the individual panels are descriptive within-recording statistics and are not used as population-level biological inference because the recordings are synthetic.

Aicumene:2026.042v2 [q-bio.NC] October 24, 2026

These auxiliary channels were not used to compute BOID. Their purpose is therefore not to provide an independent predictor of oscillator dimensionality, but to demonstrate internal state coherence of the synthetic benchmark: low-dimensional N3 and intermediate-dimensional REM epochs occur within multimodal sleep trajectories that also express the expected stage-dependent physiological organization.

Aicumene:2026.042v2 [q-bio.NC] October 24, 2026

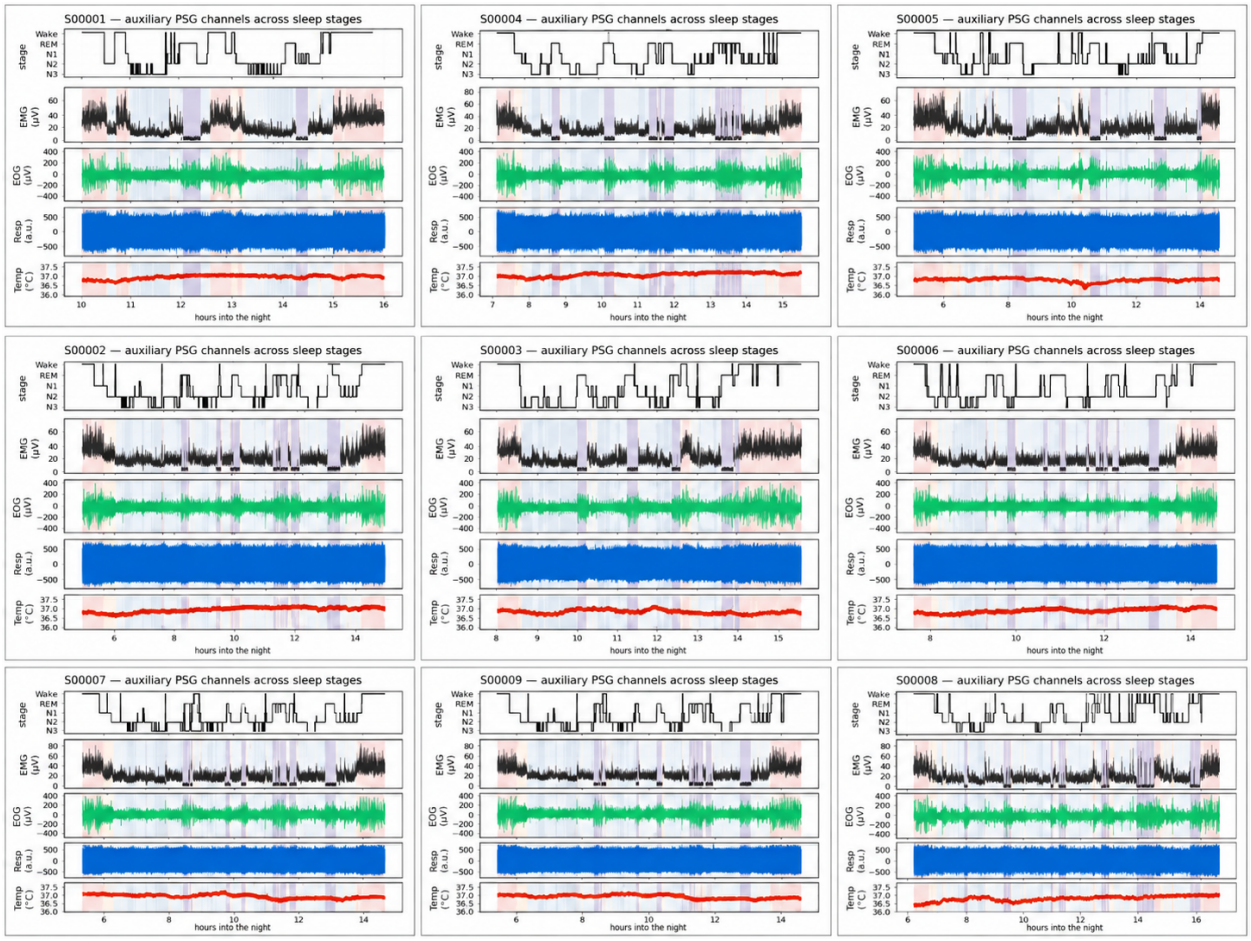

Figure S4: **Auxiliary physiological channels preserve sleep-state organization in the synthetic benchmark.** Representative synthetic recordings are shown with the corresponding hypnogram and auxiliary polysomnographic signals. From top to bottom, each panel contains sleep stage, submental EMG, EOG, respiration, and body temperature. Background shading denotes Wake (red), N1 (orange), N2 (light blue), N3 (dark blue), and REM (purple). Across recordings, tonic EMG is highest during wakefulness, decreases during sleep, and shows pronounced attenuation during REM intervals, providing a recognizable synthetic analogue of REM-associated muscle atonia. EOG and respiratory activity remain temporally structured across the night, whereas body temperature changes smoothly within the physiological range. These channels are not inputs to BOID and are shown as an internal state-coherence check of the synthetic sleep benchmark.